Quantitation of Tissue Resection Utilizing A Brain Tumor Model And 7-Tesla MR Imaging Technology.

Dan Huy Tran, B.Sc.

Experimental Surgery

McGill University, Montreal

December 2020

A thesis submitted to McGill University in partial fulfilment of the requirements of Master of Science in Experimental Surgery

TABLE OF CONTENT

Contents

ABSTRACT 6

Background 6

Objective 6

Methods 6

Results 6

Conclusion 7

RÉSUMÉ 8

Contexte 8

Hypothèse 8

Objectifs 8

Méthodologie 8

Résultats 9

Conclusion 9

ACKNOWLEDGEMENT 10

PREFACE AND CONTRIBUTION OF AUTHORS 13

ABBREVIATIONS 14

BACKGROUND 16

The history of surgical expertise and surgical education 16

Current issues in surgical training 17

Simulation and surgical training 18

Neurosurgery and artificial tumor model 20

Brain imaging: 7T MRI scan 22

Image segmentation and registration 24

Rationale for this study 27

Hypothesis 27

Objectives 27

STUDY 28

ABSTRACT 29

Background 29

Methods 29

Results 29

Conclusion 29

INTRODUCTION 30

METHODS 32

Ex-Vivo Calf Brain Models 32

Image acquisition using a 7 Tesla MRI scanner 33

Calf brain tumor model 34

Segmentation protocol 35

Registration 36

Quantification of normal brain tissue removed 37

Quantification of tumor and grey and white matter tissue resected 37

RESULTS 39

Quantification of brain tissue removed 39

Quantification of brain tumor removed 39

Calculation of total resected tumor 41

Calculation of total grey and white matter resected 41

Calculation of total tissue resected 42

Postresection structural integrity analysis of grey and white matter tracks 42

Baseline and postresection three-dimensional reconstruction views 43

DISCUSSION 43

Summary 43

Quantification of brain tissue removed 43

Alginate tumor model and quantitative analysis of tissue resections 44

Educational Opportunities: Combining Virtual Reality and ex-vivo models 45

LIMITATIONS 46

CONCLUSION 47

ACKNOWLEDGEMENT 48

FUNDING 48

DISCUSSION OF THESIS 49

Future directions 49

THESIS CONCLUSION 50

REFERENCES 52

APPENDIX 64

TABLES 64

Table 1 64

Table 2 65

FIGURES 67

Figure 1 67

Figure 2 68

Figure 3 69

Figure 4 71

Figure 5 73

Figure 6 75

Figure 7 76

VIDEOS 77

Video 1 77

ABSTRACT

Background: Animal brain models and artificial tumor models can be useful educational tools for neurosurgical residents by allowing training of bimanual technical skills. However, despite numerous models being proposed, no methodology to objectively and quantitatively assess surgical performance on present models currently exist.

Hypothesis: 7-Tesla MR scanning can be used to study surgical performances on an ex-vivo brain tumor model by comparing pre- and post-resection segmented and registered images.

Objective: First, to determine the possibility of quantifying healthy tissue removal on ex-vivo calf brains using 7-Tesla MR imaging. Second, to determine our ability to apply the methodology used in the first objective to assess artificial tumor resection on an ex-vivo calf brain model using the subpial technique. Third, to assess the accuracy of this methodology in quantifying grey and white matter along with total tissue resected during tumor removal.

Methods: Seven ex-vivo calf brains were used to develop the 7-Tesla MRI segmentation methodology. The brains were split in two groups. Three brains were used to quantitate healthy brain tissue removal using 7-Tesla segmented MRIs. Alginate artificial brain tumors were created in 4 calf brains to assess the ability of the assessed 7-Tesla MRI methodology to quantify tumor, grey and white matter removal during a subpial tumor resection.

Results: Quantitative data pointed to correlation and linearity of relationship between weights of removed healthy brain tissue and their associated volumes determined from segmented images. Analysis of pre and postoperative images of the second group of brains allowed quantification of artificial alginate tumor volumes and detection of grey and white matter tissue removed during subpial tumor resection.

Conclusion: Segmentation and registration of 7MRI images allowed for the assessment of surgical performance on an animal ex-vivo brain tumor model. This methodology can be further developed to create an educational and validation tool for surgical simulators.

RÉSUMÉ

Contexte : Les modèles animaux de cerveaux peuvent être utiles en tant qu'outils éducatifs pour les internes en neurochirurgie en leur permettant de pratiquer leurs compétences bimanuelles. Cependant, malgré la multitude de modèles présentés dans la littérature scientifique, aucune méthodologie n'existe pour évaluer la performance chirurgicale de manière objective et quantitative sur ces modèles.

Hypothèse : L'imagerie par résonnance magnétique à 7 Teslas peut être utilisée pour étudier la performance chirurgicale sur un modèle ex-vivo de tumeur cérébrale en comparant des images segmentées et recalées du cerveau animal avant et après la résection de la tumeur.

Objectifs : Premièrement, déterminer la possibilité de quantifier les masses de tissues cérébraux sains enlevés en utilisant l'imagerie par résonance magnétique à 7 Teslas. Deuxièmement, déterminer notre capacité d'appliquer cette méthodologie pour évaluer la quantité de tumeur artificielle enlevée d'un cerveau de veau en utilisant la technique de transsection sous-piale. Troisièmement, évaluer le degré de précision de cette méthodologie à déterminer les quantités de matières grises et matières blanches enlevées autour de la tumeur artificielle.

Méthodologie : Sept cerveaux de veau ont été utilisés pour développer la méthodologie de segmentation d'images par résonnance magnétique à 7 Teslas. Les cerveaux ont été séparés en deux groupes. Trois cerveaux ont été utilisés pour quantifier l'enlèvement de tissue cérébral sain à partir d'images par résonnance magnétique à 7 Teslas. Des tumeurs cérébrales artificielles en alginate ont été créées dans quatre cerveaux de veaux pour évaluer la capacité de notre méthodologie de quantifier les tumeurs, matière grise et matière blanche enlevées pendant la résection subpiale de la tumeur.

Résultats : Les données quantitatives suggèrent une corrélation et linéarité entre les masses des morceaux de tissues cérébraux sains enlevés et leurs volumes déterminés à partir d'images segmentées. Les analyses des images pré et postopératoires du second groupe de cerveaux ont permis la quantification des volumes de tumeurs cérébrales artificielles en alginate et la détection de dégâts infligés aux structures de matières blanches adjacentes aux tumeurs.

Conclusion : La segmentation et le recalage d'images par résonnance magnétique à 7 Teslas permettent l'évaluation de la performance chirurgicale sur un modèle de cerveau animal ex-vivo. Cette méthode peut être développée pour créer un outil éducatif utile et une méthode pour valider les simulateurs chirurgicaux.

ACKNOWLEDGEMENT

I would like to start my thesis by sincerely thanking my supervisor Dr. Rolando Del Maestro for giving me the opportunity to join the Neurosurgical Simulation and Artificial Intelligence Learning Centre to carry this project. I thank Dr. Del Maestro for his support every step of the way. I particularly appreciate the fact that his sincere counsel extended beyond surgical education and touched on all matters of life. I thank him for sharing with us his passion of medical history, his interest for medical innovation and his steadfast optimism for the future of surgical education. More than a supervisor, he has been a model, a person I wish to learn from and to emulate in their virtues, may they be intellectual or moral.

I would also like to thank Dr. Alexander Winkler-Schwartz, who has been kind enough to allow me to work with him in the animal operating theatre on the ex-vivo animal tumor model that he developed. Dr. Schwartz has passed on his attention for excellence, scientific rigour, but most importantly, his love for the medical profession. Beyond the scope of this thesis, he has kindly answered all the questions I addressed to him, allowing me to clearly perceive my vocation within the field of healthcare.

Four other persons were instrumental throughout the course of this thesis. First, I would like to thank Dr. Louis Collins and Dr. Houssem Gueziri for providing me with the necessary resources and knowledge to devise the segmentation and registration protocol, and for their help in collecting data. Second, I would like to thank Dr. David Rudko and Mr. Marius Tuznik for their help in scanning the brains under the 7T MRI scanner that they operate. I would like to especially thank Houssem and Marius, who have always answered my most convoluted questions with the utmost level of professionalism and kindness.

I must also extend a special thanks to the members of the Neurosurgical Simulation and Artificial Intelligence Learning Centre, who have made this year a memorable learning experience. I thank Dr. Mohammed Recai Yilmaz and Dr. Bekir Karlik for broadening my intellectual horizon, from science and healthcare to history and culture. The humanistic virtue of Science lies in its universality, which knows no borders; Recai and Dr. Karlik are two of the most eminent examples of this universality. Furthermore, I would like to thank my colleague Mr. Aiden Reich, who has joined the research group at the same time as myself. I thank him for being a good comrade in arms, not only at the Neurosurgical Simulation and Artificial Learning Centre, but also in the Surgical Innovation program. I wish him all the best moving forward with GyroClear, as the world needs more passionate and creative innovators like him. I would also like to thank Dr. Sommer Christie for her kindness and words of advice on mental health, which proved instrumental in the times when I faced significant hardship. I thank Mr. Swajan Paul for his genuine curiosity and interest in my research and wish him all the best in his journey in academia.

I would like to thank the members of my research advisory committee, including Dr. Carlo Santaguida (co-supervisor), Dr. Derek Rosenzweig (chairperson of the committee), Dr. Louis Collins and Dr. Jason Harley. Their words of advice and encouragement were instrumental in completing this manuscript

I would like to thank Mr. Nykan Mirchi, Ms. Nicole Ledwos and Dr. Vincent Bissonnette for their counsel and support throughout this year, may it be regarding work related to the thesis or advise on how to pursue a career in medicine. Their achievements and encouragements were a constant reminder that success is to be found at the end of this journey regardless of the obstacles that had to be overcome.

I would like to thank the community at the Newman Centre of McGill University for providing me with a peace haven away from home. To Father John Meehan, Father Joachim Ostermann and Mrs. Linda Diez, thank you for your kindness and wisdom which helped me at to find Christ in every interaction, conversation and cup of coffee.

Finally, I would like to thank my family, particularly my parents, for believing in me throughout my academic journey. I feel honoured and grateful to be the first one in my family to have reached such a high level of post-secondary education thanks to their support. There is no greater pride for me in life than to be the son of my parents.

PREFACE AND CONTRIBUTION OF AUTHORS

The thesis presented herein is structured in a manuscript-based manner.

The candidate led the study and performed partially or fully the following aspects of the study: data collection, image segmentation and registration, data analysis, result interpretation and writing of this manuscript.

Dr. Alexander Winkler-Schwartz operated on calf hemispheres.

Dr. Houssem-Eddine Gueziri provided advice on segmentation protocols and 3D-printed the fiducials that were inserted in the calf hemispheres.

Mr. Marius Tuznik operated the 7T MRI scanner to produce images of the brains.

Dr. Recai Yilmaz, Dr. Bekir Karlik, Mr. Aiden Reich and Mr. Swajan Paul offered their analysis and comments on the design of the experiment and on potential solutions that could be explored to analyze the MRI scans.

Dr. Rolando Del Maestro exerted oversight on the overall direction and planning of the research project. He offered advice on study design and result interpretation, notably on the need for proper quantification of brain tissue. He also contributed to the assessment of progress by identifying areas which could be improved upon.

ABBREVIATIONS

Centimeter (cm)

Coefficient of determination (R^2)

Computerized tomography (CT)

Echo time (TE)

Fast imaging with steady-state free precession (FISP)

Field of view (FOV)

Gram (gm)

Hydrogen 1 (1H)

Kilohertz (kHz)

Magnetic resonance (MR)

Magnetic resonance image (MRI)

Micrometer (μm)

Millilitres (mL)

Operating room (OR)

Phase encoding (PE)

Radio frequency (RF)

Region of interest (ROI)

Repetition time (TR)

Tesla (T)

Three-dimensional (3D)

BACKGROUND

The history of surgical expertise and surgical education

Although it is now seen as a rigorous and methodical practice, surgery has not always been held in high regards. Indeed, from the Antiquity to the Enlightenment, it was mostly seen as a trade rather than an academic discipline and, as such, was seen as inferior to medicine[1]. While medicine was practiced within elaborate intellectual and theoretical frameworks developed over centuries, surgery was largely a technical trade due to a lack of understanding of human physiology and anatomy[2]. Although human dissections were recorded as early as the Hellenistic period with dissections performed by Herophilus and Erasistratus of Alexandria in the 3rd century BC[1, 3], they remained quite rare due the taboo in Ancient Greece and Rome on dissecting human corpses, as it was perceived as a transgression of a free man's dignity and integrity. Middle-Age surgeons in the Muslim world further explored human anatomy but in Western Europe, surgery remained static for centuries despite the relaxation in the ban on dissection in northern Italian city-states[2, 3]. In medieval Europe, universities trained surgeons in a limited range of minor operations; yet, high demand in surgical procedures allowed the coexistence of barber-surgeons besides university-trained surgeons[2, 4]. These barber-surgeons carried operations ranging from bloodletting to amputations. The lack of sanitation and the resulting poor outcomes led to their unfavorable reputation, and by extension, to the unfavorable reputation of surgery overall.

Despite the works of Renaissance surgeons such as Andreas Vesalius and Amboise Paré, it was not until the Enlightenment that surgery began to be a scientific and academic discipline thanks to the work of John Hunter. Hunter laid the foundations for experimental surgery through rigorous studies of specific anatomical systems[5]. He spearheaded the concept of scientific

surgery, that is, surgical knowledge based on direct observation and experimentation, as illustrated by his work on the lymphatic system[5]. The work of Hunter and his contemporaries established surgery as an evidence-based medical discipline; surgery no longer remained in the realm of speculation and theories derived from dissections on animals and became an integrant part of medicine. The next crucial step in the foundation of modern surgery was the establishment of residency programs at John Hopkins Hospital by Dr. William Halsted. He had studied in Europe under the supervision of German and Austrian surgeons such as Theodor Billroth. Halsted brought back to America this knowledge and devised a learning programme based on the "see one, do one, teach one" principle[6, 7]. Under this principle, residents were required to observe a senior surgeon perform surgeries and replicate the skills they had observed, after which they were required to demonstrate their knowledge by teaching fellow students what they had learned. This training method was meant to give residents the opportunity to gain responsibility as they gained experience through a process of "graduated responsibility".

Although innovative at the time, this model came to be questioned; not only was surgery an experimental field where mistakes commonly occurred[8], but it was also not under the significant public scrutiny. Recently, the rise of societal expectations on improved medical practice and ethics combined with the increasing number of students has led to more standardization of medical teaching and less time for graduated responsibility. These changes have tilted the balance in favour of increasing patient safety, thus resulting in a shift in the surgical training paradigm.

Current issues in surgical training

Surgical training has undergone profound changes as educators sought to train surgeons in a more standardized and effective learning environment. First, as growing concerns on the

well-being of trainees increased, measures were taken to limit burnout and mental health strains on residents[9]. For instance, residents in the USA cannot work more than 80 hours a week[10]. With a decrease in the amount of time spent on training, curricula were developed with the assumption that a resident would reach full competency by the end of their residency[11]. Second, the last decades have seen an increase in neurosurgical cases being brought to court[12-14]. Indeed, neurosurgery is the surgical field with the highest number of litigations in the US, with nearly 34% of surgeons defending in court practice neurosurgery[13]. These concerns lead not only to surgeon burnout but to the higher cost of patientcare [15]. Third, because of the intensive nature of the training and the limited number of spots available in surgery residency programs, only a small number of surgeons are trained every year. This highlights the need to develop methods to improve surgical training and patient outcomes. To address some of these issues, there has been a focus on the growth of simulation technologies to train surgeons in a safe, controlled and stress-free environment[16]. Finally, from a point of view of surgical expertise, studies have suggested that surgeons continue to improve their level of expertise after fellowship, consistent with a continuing learning curve[11]. Key opinion leaders in the field have advocated for the development of new training curricula that would allow residents to train more efficiently so that they would reach both competency and expertise earlier in their career. The push to tackle the historical need for simulation methods in surgical training continues to increase with new technologies being proposed[17-27].

Simulation and surgical training

Simulation as an educational tool has a long history in almost all fields of human activity. For instance, Prussian officers in the 19th century were instructed in the art of maneuvering armies through playing *Kriegsspiel*, a wargame through which officers could learn to effectively

use topography, tactical positioning of troops and detection of enemy movement. In surgery, the most realistic form of simulation has always been dissection on cadavers[25]. Such dissections were recorded as early as the Hellenistic period with the dissections of Herophilus and Erasistratus of Alexandria in the 3rd century BC[1]. Surgical simulation can take many forms, including physical models, augmented reality and virtual reality[17-25]. While physical models have historically been the most common, the advent of computing technologies has allowed for the development of sophisticated simulators such as virtual reality simulators. Simulators are considered a safe way of training surgeons on high-risks scenarios that could lead to dangerous outcomes if carried on actual patients. This phenomenon in surgery is inspired from the use of simulators in other high-risks fields such as aeronautics, where pilots must train on simulators for a set amount of time before they can step foot in a pilot cabin[28]. The rationale behind the use of simulators is clearly defined; using simulators allows for trainees to learn from their mistakes and to see the unfortunate outcomes that may arise should an operation not be carried out properly. This rationale has been validated by the trainees themselves, who report high levels of satisfaction with using simulators as they can safely train and reflect on their performance with instructors in a safe and productive manner. Several platforms and simulation systems exist to cover the wide range of surgeries carried in hospitals. One such platform is the NeuroVR (formerly NeuroTouch, CAE Healthcare, Montreal, Quebec, Canada), which allows users to train on different operative scenarios including subpial brain tumor resection[29, 30].

Despite their high level of fidelity to real-life conditions, simulators have inherent limitations that prevent them from fulfilling all the formative role of live operative conditions. First, only a handful offer the full range of sensory feedback that would be available in a real OR setting. These feedbacks include 3D visuals, sound and haptics. Developing a simulator that

includes such features require both engineering and medical expertise. This makes the development of such machines an expensive process. Second, once the simulators have been developed, realistic and educationally relevant surgical scenarios must be developed to fully take advantage of the features of the simulator. Medical experts are critical to define the important features of a given surgical procedure which needs be included in the simulation and to assess the realism of the simulation scenario once it has been developed. While some surgical procedures are straight forward and divided in clearly defined steps, others are more variable, including complex brain tumor resection. Indeed, tumor resection is a continuous process in which the neurosurgeon removes brain tumor throughout the tumor operation[31, 32]. This operative mode contrasts with operations found in other surgical fields, such as anterior cervical discectomy and fusion in orthopaedic surgery, in which each step must be completed before moving on to the next one in a clearly defined succession of steps. Third, simulators come at a high price, which makes their use prohibitive in certain settings. As the current global trend is to decrease spending in most public health care system, only a handful of hospitals in the world can afford to equip themselves with enough simulators to make them worth the investment needed to acquire and deploy them.

Neurosurgery and artificial tumor model

While simulators advantages and disadvantages as discussed above, the current literature continues to outline their potential and foresees this technology becoming conventional education tools[16, 24, 25, 33]. To reach that point, the use of simulators must first be validated. The most effective validation for a simulator is to quantitatively demonstrate the positive effect of simulator training on students' surgical performance. In the context of neurosurgery, measuring students' surgical performance on live human operations has many limitations[34]. Thus, the use of

ex-vivo physical brain models as proxies for human brain disorders to assess students' surgical skills is one methodology to quantitatively assess students' performance. One experimental methodology would be a single-blinded 2-armed randomized control trial to assess the effect of simulation training on the primary outcomes such as volume of brain tumor and normal tissue resected. Common ex-vivo animal brain tumor models include the use of bovine, porcine and ovine systems. Their popularity as models stems from their availability, their low cost and the degree of realism they offer. Porcine and ovine brains are significantly smaller compared to human brains, which limits their usefulness[35]. Bovine ex-vivo calf brains are in the same size range as human brains and were selected at the Neurosurgical Simulation and Artificial Intelligence Learning Centre as the appropriate proxy for human brain models[34]. Using ex-vivo calf brains, it is possible to select gyri and sulci in the parietal region which mimic the human brain.

Once the animal model has been selected, various biomechanical, anatomical and surgical issues can be integrated to create a realistic simulation. In the field of oncological neurosurgery, one subject of interest is the creation of artificial brain tumor models which can provide trainees exposure to the challenges associated with tumor resections in a safe and controlled no risk environments. Certain tumors such as high-grade gliomas are difficult to completely resect due to their high vascularization and the presence of cancerous cells outside the area seen on the MRI mages. The techniques used to resect these complex tumors are demanding to perform and difficult to master[32]. A surgical method that is used for complex human tumor removal and epilepsy procedures is the subpial resection technique, which allows for preservation of vascularization in the adjacent normal gyrus and is associated with improved surgical outcomes[31]. Various artificial tumor ex-vivo models have been proposed using a range

of different material to imitate the appearance and stiffness properties of real tumors; such substances include agarose food sugar[22, 23], silicone[26], fibrin glue[18] and polymer resins[17, 19, 21]. All these reported models lack quantitative assessments of tumor stiffness properties which would allow these artificial tumors to be more adequately compared to the stiffness of human brain tumors and provide equivalent haptic feedback. These ex-vivo studies also do not quantitatively assess surgical performance based on the removal of peritumoral removal of normal grey and white matter associated with the tumor resection procedure.

A new brain tumor model was developed by Winkler-Schwartz et al. utilizing stiffness data collected from human brain tumors and incorporated these human brain tumor stiffness values into an artificial alginate tumor model using a ex-vivo bovine calf tumor system[34]. This model was used in these studies for objective assessment of tumor resection volumes along with grey and white matter removal during the subpial resection of the tumor. A quantitative analysis methodology was developed using 7-Tesla MR scans of the model developed by Winkler-Schwartz et al. to assess tumor resection volumes along with grey and white matter removal during the subpial resection of the artificial alginate tumors.

Brain imaging: 7T MRI scan

The general lack of analytical protocols associated with current brain tumor models prevents surgical instructors from objectively quantifying and analysing surgical performance[16-22]. Neurosurgeons in the clinical setting make frequent use of brain imaging technologies such as computed tomography (CT) and magnetic resonance imaging (MRI) scans to plan and assess the results of a tumor operative procedure. These imaging technologies can be used to assess a wide array of parameters, including vascular properties of the brain, presence of tumor, infection,

inflammations, lesions and trauma. This wealth of information is accessible to neurosurgeons upon visual inspection of scans.

The principle of MRI takes advantage of the presence of water within tissues. Applying a strong and uniform external magnetic field on the body using a magnet causes hydrogen protons of water molecules to align along their axes, which creates a magnetic vector aligned along the axis of the MRI scanner[36, 37]. Next, the alignment of these protons is disturbed by a radio frequency (RF) pulse that is emitted from RF coils present in the scanner. Once the radio frequency is turned off, the protons emit a radio wave as they relax. The emitted radio signal is then picked up by receiver coils present throughout the scanner. It is important to note that the strength of the external magnetic field can be altered in such a way that different slices of the body resonate depending on the properties of the magnetic field. To do so, scanners are equipped with gradient coils which alter the magnetic field in increments. The intensity of all emitted radio signals across all slices is plotted into a series of grey scale images, thus allowing for image reconstruction of a 3D volume of the scanned object. To highlight different anatomical structures, two different parameters can be used. The first one is the echo-time (TE), which is the time between the emission of an RF pulse and the reception of its corresponding echo. The second one is the repetition time (TR), which is the time between two successive pulses applied to a same anatomical slice. By varying the lengths of these two parameters, different weighted images can be obtained, with T1-weighted images having short TE and TR while T2-weighted images have long TE and TR. T1 and T2 are time constants describing two different relaxation properties of tissues, which are respectively “spin-lattice relaxation” and “spin-spin relaxation”[37].

Although MRI is now widely used in clinical settings, an important challenge remains. Because full polarization of all photons within the scanned sample is virtually impossible to

achieve, MRI are prone to high noise levels which affects the signal-to-noise ratio (SNR). This is a result of incomplete spin polarization of a scanned body – it is virtually impossible to get all photons to align along the external magnetic field. To tackle this issue, two approaches exist to induce more spin polarization within the scanned body. First, hyperpolarization can be induced by injecting different sorts of substances within the body including the stable isotope carbon 13[38, 39]. Second, and more commonly, the strength of the external magnetic field can be increased to increase spin polarization. Higher magnet strength offers the advantage of increasing SNR and contrast-to-noise ratio (CNR)[37, 40, 41]. Because of the accuracy at which it allows data acquisition and subsequent image segmentation and registration, the 7T MRI scan system has been chosen to acquire scans of ex-vivo calf brains with and without the artificial brain tumor developed at the Neurosurgical Simulation and Artificial Intelligence Learning Centre[34].

Image segmentation and registration

Image segmentation is a common process in computer vision through which a digital image is divided into various segments based on specific criteria. The goal of segmentation is to process an image to make the image more meaningful and analytical by having a whole set of segments covering the entire picture. In medical imaging, these segments act as labels to denotate specific anatomical structures that could otherwise be hard to recognize to the untrained eye. Segmentation is often used to create 3D reconstructions of anatomical structures by putting together a set of images that have been segmented[42]. Such 3D reconstructions are typically shown as volume rendering, that is, a 2D projection of a 3D scalar field. This offer many benefits to clinicians, including the ability to track the progression of a disease over time[43, 44].

Because of its many applications, segmentation can be performed in many ways. Segmentation can be performed based on multiple criteria including image intensity, color, edges

and texture. It can be done manually, semi-automatically or automatically[42]. In medical imaging, manual segmentation is a method involving a skilled technician manually highlighting anatomical structures of interest. Although it remains the gold standard in medical imaging, it is subject to variability in accuracy[42, 45, 46]. Over the past two decades, an increasing body of literature has been published on the development of automatic segmentation methods, where segments are automatically assigned by the software based on statistical or probabilistic models[47-51]. Such methods include atlas-based segmentation, model-based segmentation, region-based segmentation, amplitude segmentation and edge-based segmentation[50] . While these methods allow for a high throughput of data processing, it requires the previous analysis of vast amount of data before a model, atlas or algorithm can be proposed[52]. Furthermore, despite recent advances in the field, it is still an error-prone method, thus limiting its application to clinical settings. In semi-automatic segmentation, users are required to give minimal input before the software performs the segmentation according to the highlighted method[53], producing a segmentation which can be as accurate as a manual segmentation but faster[54], yet still slower than fully automatic segmentation[55]. Such methods include Otsu thresholding[56], growing from seeds[57] and smoothing[58]. To supplement such segmentation of MRI scans, a straightforward registration process of pre and postoperative segmented scans would enable instructors to perform a comparative assessment of both scans and to determine the quality of the surgical procedure[59, 60].

Although this MRI methodology is available, the ex-vivo animal tumor models used as educational tools did not assess normal grey and white matter removal durng operative procedures. The development and use of segmented medical images on these models presents numerous advantages which can be translated for patient care. First, animal brain models

equipped with the proper analysis methodology can serve as validation for simulators like the NeuroVR by enabling instructors to track the progress of students as they train on the simulator. Second, it would give both trainees and instructors objective data which they can analyze to adjust the trainee's learning and focus on specific skills to improve. Third, from a point of view of patient care, the necessity to monitor tumor growth over time requires surgeons to be able to monitor such growth and to adapt their treatment accordingly[61]. Introducing segmentation of medical images like 7T MRI scans would allow surgeons to supplement their analysis with quantitative data. Although the current methodology remains time-consuming manual segmentation performed by skilled technician, advances in computer vision and development of new automatic processing pipelines may eventually allow for the systemic use of segmented images as standardized tools for clinical assessment.

Rationale for this study

The following study proposes a methodology to quantitatively and visually analyse surgical performance utilizing 7-Tesla MR segmented scans of ex-vivo calf brains containing alginate tumors.

Hypothesis

7-Tesla MR scanning can be used to study surgical performances on an ex-vivo brain tumor model by comparing pre- and post-resection segmented and registered images.

Objectives

The aims of this pilot study were to: 1) To determine if the assessment of baseline images and postresection images acquired using 7-Tesla MRI scanner can accurately quantitate normal brain tissue removed in a calf brain model, 2) To assess if baseline and postresection 7-Tesla MR imaging technology can quantitate alginate brain tumor resected after subpial resection in a calf brain model and 3) To outline if baseline and postresection 7-Tesla MR imaging technology can quantitate grey matter, white matter and total tissue resection following subtotal and total subpial resection of alginate brain tumor in a calf brain model.

STUDY

Quantitation of Tissue Resection Utilizing A Brain Tumor Model And 7-Tesla MR Imaging Technology.

Dan Huy Tran, BSc, Alexander Winkler-Schwartz, MD, Marius Tuznik, MSc, Houssem-Eddine Gueziri, PhD, David A. Rudko, PhD, Aiden Reich, BEng, Recai Yilmaz, MD, Bekir Karlik, PhD, D. Louis Collins, PhD, Adrian Del Maestro, PhD, Rolando Del Maestro, MD, PhD

The preceding work incorporates supplemental material to provide a more thorough overview of the methodologies used and results obtained.

Manuscript under review in World Neurosurgery

ABSTRACT

Background: Animal brain tumor models can be useful educational tools for the training of neurosurgical residents in risk-free environments. MRI technologies have not been employed utilizing these models to quantitate tumor, normal grey and white matter and total tissue removal during complex neurosurgical procedures. This pilot study was carried out as a proof of concept to demonstrate the feasibility of using brain tumor models combined with 7-Tesla MR imaging technology to quantitatively assess tissue removal during subpial tumor resection.

Methods: Seven *ex-vivo* calf brain hemispheres were employed to develop the 7-Tesla MRI segmentation methodology. Three brains were used to quantitate brain tissue removal employing 7-Tesla MRI segmentation methodology. Alginate artificial brain tumor were created in 4 calf brains to assess the ability of 7-Tesla MRI segmentation methodology to quantitate tumor, grey and white matter along with total tissue volumes removal during a subpial tumor resection procedure.

Results: Quantitative studies demonstrated a correlation between removed brain tissue weights and volumes determined from segmented 7-Tesla MR images. Analysis of baseline and postresection alginate brain tumor segmented 7-Tesla MR images allowed quantification of tumor, grey and white matter along with total tissue volumes removed and detection of alterations in surrounding grey and white matter.

Conclusion: This pilot study demonstrated that the use animal tumor models in combination with 7-Tesla MR imaging technology provides an opportunity to increase the granularity of data obtained from operative procedures and improve the assessment and training of learners.

INTRODUCTION

Surgical technical skills education is evolving from a time-focused apprenticeship towards a quantifiable competency-based model.[7] Competency in bimanual psychomotor performance in neurosurgery may be considered to have been achieved when the trainee can safely and efficiently perform a variety of procedures utilizing appropriate surgical techniques.[62] The subpial resection procedure allows neurosurgeons to resect brain tumors and epileptic foci which border on important cortical structures while minimizing injury to adjacent pial-lined gyral tissues and hemorrhage from subpial vascular structures.[27, 31] Maintaining pial layer integrity is associated with better postsurgical patient outcomes and is an important bimanual technical skill for surgical trainees to master.[31] Studies on virtual reality neurosurgical simulators with haptic feedback highlight the importance of quantitating simulated subpial resection skills performance. Normal grey and white matter tissue along with tumor volume resection associated with subpial resection, force application[63-68], tool acceleration[69], bimanual dexterity[68, 70-72] and impact of stress[72] have all been employed to assess level of expertise on these simulators.[73] Linking neurosurgical psychomotor bimanual skill performance in virtual reality simulators scenarios to resident specific training in operating room environments continues to be challenging. There is a need to outline models which can accurately quantitate both technical psychomotor skills and operative results in realistic operative setting with comparable virtual reality simulator resident evaluations on similar scenarios. These models need to possess both visual and tactile reality and be coupled with advanced quantitation MRI methodology. An animal model allowing quantitative assessment of surgical performance during the subpial resection for tumor procedures would be important adjuvant in competency-based surgical education. Analytical MRI protocols based on the comparative analysis of baseline and postoperative images of

patients are common but do not allow quantitative assessments of psychomotor performance during complex procedures such as subpial resection.[42, 44] Although automatic methods exist to carry out these studies, manual segmentation delimitating abnormal tissue contours is also employed and remains the gold standard.[42, 45, 46] To make this method more efficient, semi-automatic tools exist which require decreased user input to perform these tasks.[53-58] These MR technologies have not been employed utilizing animal models to quantitate normal grey and white matter removal to improve access for tumor resection along with resultant tissue injury. The authors have developed a framework whereby neurosurgical performance and extent of resection has the potential to be accurately quantified in a controlled setting utilizing an ex-vivo calf brain artificial alginate tumor model[34]. This framework allows manual and semi-automatic brain segmentations on baseline and postresection MRIs. Images are acquired on a 7-Tesla MRI scanner to optimize image registration and to carry out quantitative analysis of normal tissue and brain tumor resected volumes during the utilization of the subpial technique[34]. 7-Tesla MRI was chosen over 3-T MRI for its increased spatial resolution, thus allowing for better resolution of subtle landmarks in brain tissue.[74, 75] High spatial resolution was critical in producing accurate segmentation of MRIs, thus increasing the accuracy of the subsequent MRI registration. This pilot study was carried out as a proof of concept to demonstrate the feasibility of using brain tumor models combined with 7-Tesla MR imaging technology with the aim of verifying that the union of these methodologies is both a feasible and practical application in the quantitation and understanding of complex neurosurgical skills.

The aims of this pilot study were to: 1) To determine if the assessment of baseline images and postresection images acquired using 7-Tesla MRI scanner can accurately quantitate normal brain tissue removed in a calf brain model, 2) To assess if baseline and postresection 7-Tesla MR

imaging technology can quantitate alginate brain tumor resected after subpial resection in a calf brain model and 3) To outline if baseline and postresection 7-Tesla MR imaging technology can quantitate grey matter, white matter and total tissue resection following subtotal and total subpial resection of alginate brain tumor in a calf brain model. To our knowledge, this is the first study to employ a brain tumor model and 7-Tesla MRI technology to gain insight into quantification of specific tissue resection during a complex neurosurgical procedure.

METHODS

Ex-Vivo Calf Brain Models

Seven fresh *ex-vivo* calf brain cortical hemispheres were utilized for these studies since they structural resemble human brain, are low cost and small enough (about 150 grams) to fit into the 7 Tesla MRI coil (Figure 1A)[34]. The calf hemispheres were separated into 2 groups. Group 1 included 3 hemispheres which were utilized to assess if comparing baseline and postresection 7-Tesla MRIs can quantitate normal brain tissue removed. Initial baseline scans were carried out before tissue resection (Figure 1 C). In total, 6 brain segments of increasing sizes were resected from 3 calf hemispheres (Figure 1B). All resected brain segments were weighed (High Precision Scale, Smart Weight Ltd, Changzhou, China). Calf hemispheres with resected segments then underwent a postresection scan (Figure 1D). In Group 2, the cortical grey matter gyri of 4 calf hemispheres were utilized to create alginate artificial tumors of different sizes. Baseline 7-Tesla scans were then carried out. Following this scan, the neurosurgical resident operator was given specific instruction on how to perform a subpial resection of the overlying cortical grey matter tissue and tumor with minimal injury to underlying white matter tracks. Following procedural completion, postresection scans were performed. Group 2 was used to assess if our pipeline of segmentation and registration of 7-Tesla MRIs can quantitate percentage of alginate brain tumor

resection, quantitate grey and white matter removed and total tissue resected during the subpial procedure in the calf model. The McGill University Health Centre Research Ethics Board, Neurosciences-Psychiatry approved these studies.

Image acquisition using a 7 Tesla MRI scanner

Before baseline scans, 3D printed polylactic acid fiducials were inserted into all 3 calf hemispheres in Group 1, and 1 of 4 calf brains in Group 2 (Figure 2 A and B). The fiducials were used to assess their usefulness during registration of baseline and postresection images. Calf hemispheres were placed in a cylindrical container and covered with an MR-invisible fluorinated solution, FC-40 (Sigma Aldrich, St. Louis, Missouri).

In this study, 1H-MR scans at resonance frequency of 300MHz were carried using a Bruker Pharmascan 7 T MRI scanner with an AVANCE II radiofrequency (RF) amplifier system and a BFG-150/ 90-S gradient system. (Bruker Biosciences, Billerica, MA). The plastic tubes containing the brain hemispheres were imaged inside a cylindrical RF transceiver coil with an inner diameter of 6 cm. The sequences were run using the Burker's proprietary imaging software ParaVision 5.1. For each brain hemisphere, the same scanning protocol was performed to obtain baseline MRIs and postresection MRIs.

All 3 brains of group 1 were scanned using a 3D Fast Imaging with Steady-state free Precession (FISP) sequence with: echo time (TE) = 5 milliseconds, repetition time (TR) = 10ms; scan repetition time = 4000 milliseconds, receiver bandwitdth = 50kHz, flip angle = 30 degrees, axial FOV = 6cm × 5.25cm × 5.1cm, voxel resolution = 200 μm, matrix size = 300 × 255 × 255. Twenty-four averages were acquired making for an anticipated total scan time of approximately 12 hours. Parameters were adjusted to determine the set of geometric parameters that represented the most optimal trade-off between spatial coverage and scan time. Indeed, the parameters had to

produce a field of view (FOV) that encompassed the entire tumor in each brain while ensuring that each scan would not exceed reasonable periods of time. All 4 brains of group 2 were scanned using a 3D FISP sequence with TE = 5ms. The following parameters were common to all 4 brains of Group 2: TR = 10 milliseconds, scan repetition time = 4000 milliseconds, receiver bandwidth = 50 kHz, flip angle = 30 degrees. The differences in protocol between the four brains included the field of view, matrix size, resolution and anti-aliasing. The resolution for brains 1, 2 and 3 was 150 µm and the resolution for brain 4 was 200 µm. **Brain 1**: axial FOV = 4.8cm × 4.5cm × 3.3cm, matrix size = 320 × 300 × 220. **Brain 2:** axial FOV = 5.25cm × 5.25cm × 3.3cm, matrix size = 350 × 350 × 22. **Brain 3:** sagittal FOV = 6cm × 5.1cm × 5.1cm, matrix size = 300 × 255 × 255. **Brain 4:** coronal FOV = 5.70cm × 5.25cm × 2.64cm, matrix size = 380 × 350 × 176.

Calf brain tumor model

The created artificial tumor consisted of a 2% weight by volume (W/V) Algin I-1G Alginate (KIMICA Corporation, Tokyo, Japan) and a calcium sulfate solution (final calcium concentration in the alginate 12 mM) along with a 10 times dilution of gadolinium solution, Gadobutrol (Bayer AG, Leverkusen, Germany) as previously described by Winkler-Schwartz et al[34]. Alginate tumor stiffness was optimized based on data obtained from human tumor samples and food coloring (Club House, McCormick & Company, Inc, MD, United States) was added to simulate realistic brain tumor color. The alginate, calcium and gadolinium mixture were injected at a subcortical depth of 5-7 millimetres into the grey matter of a cortical gyrus to standardize tumor location[34]. After baseline 7-Tesla MR scan completion, the hemisphere was inserted into a plastic receptacle mimicking the shape of a human skull with surgical towels lining the surgical wound to replicate the human operating room environment. The gyrus region containing the

tumor which was to be resected by the operator was outlined with black marker (Figure 2B). In an animal operative room brain tumor resection was carried out using a subpial technique using micro-scissors to incise the pia mater, a bipolar coagulator to lift the pia and a Sonopet ultrasonic aspirator (Stryker, Kalamazoo, MI, USA), to remove normal cortical grey matter overlying and surrounding the artificial brain tumor visualized through an OPMI Pico surgical microscope (Carl Zeiss Co., Oberkochen, Germany) (Figure 2C and D). A sample operation of the subpial resection technique can be viewed in video 1 from reference 26. After the operator felt that the tumor had been completely removed the brain then underwent a postresection 7-Tesla MR scan.

Segmentation protocol

Each pair of baseline and postresection 7-Tesla MRIs of each group was processed using the software **3D Slicer 4.10.2.**[76] The N4ITK bias field correction filter was used to normalize the signal inhomogeneity in each volume, which was particularly necessary for volumes of Group 2 due to gadolinium hyperintensity. This image filtering process does not require prior tissue classification.[77, 78] After filtering, a combination of manual and semi-automatic segmentation methods was performed to assess the volumetric differences between baseline and postresection MRIs of calf hemispheres. Tissue types were defined as cerebral cortex, cerebral white matter and artificial tumor; each tissue type was assigned a specific segment. Additional segments included fiducials and air. Each segment was assigned a specific color code, which was consistent across all MR volumes. The segmentation process was divided in two parts. First, white matter tracts were manually contoured by hand for improved accuracy. Image contrast was adjusted throughout the white matter segmentation process to highlight different sections of white matter tracts, such as borders between grey and white matter or white matter tracts directly adjacent to hyperintense tumor. Once white matter tracts were manually segmented, grey matter regions were segmented

manually with level tracing around the white matter segment. Tumors were then automatically segmented using the Otsu's thresholding method.[56] For each brain volume, 20 to 30 slices were individually segmented, after which a semi-automatic growing seed function[57] was used to extend the segmentations to all slices. Air and ventricles were then automatically segmented using the Otsu's thresholding method[56] and removed from the final segmentation. Finally, for greater anatomical accuracy, median smoothing with a 0.50-millimetre kernel size (3x3x3 pixels) was applied for white matter segments and grey matter segments.

Registration

Once segmentation was performed, postresection segmented images were registered onto the matching baseline segmented images to visualize the geographical location where resection occurred. This was done using the 3D Slicer extension "Segmentation registration"[79]. The baseline segmentation and image were kept fixed as the matching postresection segmentation and image were displaced and deformed such that relevant anatomical landmarks from these brains matched their counterparts on the baseline brain. To account for deformation, several baseline brains had fiducials inserted to help in defining landmarks for registration. Registration occurred in multiple steps. First, when present, fiducials were registered using a rigid transformation of the postresection images. Second, if necessary, the postresection segmentation and image underwent another rigid transformation using white matter as the moving segments. If the postresection shape of the brain was significantly different from baseline upon visual inspection, cerebral cortex underwent a deformable transformation. For each of the segments previously mentioned, registration was performed only once to reduce the amount of deformation of the postresection segment. Following registration, a region of interest (ROI) was delimitated around the resected and operated regions to define the boundaries for the extraction

of volumetric information. ROI delineation varied across brain hemispheres depending on the level of deformation of each hemisphere. In Group 1 hemispheres, the ROIs were concentrated around the resection sites. In Group 2 hemispheres, because the injection of the alginate artificial tumor caused deformation of adjacent brain structures, the ROIs were expanded to encompass the tumor and its immediate surrounding. In brain 3 of Group 2, the deformation was such that the ROI encompassed the entire section of the brain containing the tumor.

Quantification of normal brain tissue removed

In the 3 Group 1 hemispheres, predetermined segments of brain tissue were removed after the baseline scan which was followed by a postresection scan. Quantitative information of each segment was available in the form of tables containing the segments statistics for each volume. Each table contained two sets of information, the segments statistics for the entire volume and the segment statistics for the region within the boundaries of the ROI. These tissue volumes were reported in millilitres. Differences in tissue volume between baseline and postresection images were calculated based on the segment statistics for each ROI. A linear model was created and used to predict the weight (in gm) of the removed tissue based on the tissue volume removed derived from the 7-Tesla MRIs segmentation and registration results (Figure 3).

Quantification of tumor and grey and white matter tissue resected

All volumes are reported in millilitres. In a calf hemisphere without the presence of a tumor following image segmentation and registration, the total baseline volume (*ROI)* would be composed of total grey matter volume (N_g) and total white matter volume (N_w)which may be represented as:

$$ROI = N_g + N_w \quad (1)$$

In Group 2, following image segmentation and registration, a ROI on the baseline scan containing the tumor was outlined (Figure 4A). The total baseline ROI volume is composed of total grey matter volume (N_g), total white matter volume (N_w) and tumor volume (N_t) Therefore, the total ROI volume which contains the tumor may be considered as:

$$ROI = N_g + N_w + N_t \quad (2)$$

The subpial removal for tumor involves resection of overlying grey and surrounding white matter along with the tumor amount removed. On the postresection images, the previously identified ROI on the baseline scan is composed of residual grey matter volume ($N_{g'}$), residual white matter volume ($N_{w'}$), residual tumor volume ($N_{t'}$)) and total resected tissue volume (N_r), seen as empty space:

$$ROI = N_{g'} + N_{w'} + N_{t'} + N_r \quad (3)$$

The change in grey matter volume (ΔN_g) between the baseline and the postresection scan is the difference between the baseline grey matter volume (N_g) minus the residual grey matter volume ($N_{g'}$) after resection:

$$\Delta N_g = N_g - N_{g'} \quad (4)$$

The change in white matter volume (ΔN_w), which is the total volume of white matter resected, is the difference between the baseline white matter volume (N_w) minus the residual white matter volume ($N_{w'}$) after resection:

$$\Delta N_w = N_w - N_{w'} \quad (5)$$

The change in tumor volume (ΔN_t), which is the total volume of tumor resected, is the difference between the baseline tumor volume (N_t) minus the residual tumor volume after resection ($N_{t'}$):

$$\Delta N_t = N_t - N_{t'} \quad (6)$$

The total resected tissue volume (N_r) can be calculated from the following equation:

$$N_r = \Delta N_g + \Delta N_w + \Delta N_t \ (7)$$

Therefore, equation 7 allows for the calculation of the total resected tissue volume N_r during the procedure.

RESULTS

Quantification of brain tissue removed

Six brain segments of increasing sizes were removed from the 3 calf hemispheres in Group 1. Two small segments (0.17 and 0.54 gm) could not be accurately identified on the postresection segmented images due to distortions associated with placing the postresection brain into the tube necessary for 7-Tesla MR imaging. Four brain segments could be assessed (Table 1). Linear fitting of the data yielded a predictive model $p(x) = 0.9373\ x + 0.0576$. A correlation coefficient of 0.9987 and a coefficient of determination (R^2) of 0.9974 were established. The polynomial model can predict up to 99.74% of the variance in recorded weights (Figure 3). Volumetric data in millilitres of tissue removed when comparing baseline and postresection segmented images were analysed using the developed polynomial model and the predicted error ranged from 0.11 to 7.58% (Table 1). These results suggest that the 7-Tesla MRI techniques outlined can accurately predict small brain segment removals when deformation between baseline and postresection segmented images is not too significant. When the ROI on the postresection scan can be accurately delineated, the polynomial model can determine the brain tissue weights when larger amounts of brain are removed.

Quantification of brain tumor removed

Four calf hemispheres were injected with alginate tumor ranging from 0.5 to 1.5 millilitres (Table 2). The alginate tumors were easily identified on the baseline coronal 7-Tesla MRIs and segmented coronal images because of the presence of gadolinium (Figure 4). Postresection

sagittal segmented images demonstrated complete tumor removal in 3 of 4 tumors studied (Figure 5). The coronal and sagittal segmented images of the baseline scan show the presence of the injected alginate tumor in the grey matter gyrus (Figure 4 and 5). The area of tissue resection, involving grey matter, white matter and tumor can be appreciated when comparing the detailed baseline and postresection coronal and sagittal segmentation images available. Injection of increased millilitres of alginate was associated with tumors of increased volume (Table 2). Baseline segmented sagittal images demonstrated tumors of irregular form and different shapes (Figure 5A, C, E, and G). In brain 1, the tumor resection was subtotal; very little grey matter overlying the tumor appeared to have been resected (Figure 5B). In postresection sagittal segmented images of brains 2 and 3, the overlying grey matter and a portion of white matter have been removed during the resection (Figure 5D and F). In the postresection image of brain 3 outlined in Figure 5F, the subpial grey matter resection appears incomplete, leaving irregular areas of grey matter in the resection cavity. In Figure 5H, the postresection cavity of brain 4 is severely compressed, leaving no resection cavity and thus preventing an assessment of baseline grey (N_g) and white (N_w) matter removed tissue using our registration method. The ROI on a baseline coronal segmented image of a calf brain hemisphere containing an irregular tumor is delineated (Figure 6A). Both grey (N_g) and white (N_w) matter tissue are outlined in a detailed coronal segmented view of the ROI in which no tumor is present (Figure 6B). A baseline coronal segmented image of the ROI containing a complex irregular tumor is also shown (Figure 6C). Grey (N_g) and white matter (N_w) along with tumor (N_t) are outlined. On the postresection segmented coronal image, residual grey matter $(N_{g\prime})$, residual white matter $(N_{w\prime})$ along with the residual tumor regions $(N_{t\prime})$ in the equivalent ROI location as on the postresection image can be identified (Figure 6D). An area of resected tissue can also be identified as empty space along

with what appears to be tissue injury to grey matter and white matter structures involving adjacent gyri.

Calculation of total resected tumor

In 3 of 4 calf hemispheres containing tumors operated on, 100% of the tumor was removed since no residual tumor could be visualized on the postresection images (Table 2). In the experiment in which postresection residual tumor was seen (brain 1), equation 6 was used to calculate the change in tumor volume (ΔN_t) between the baseline and postresection. This was possible since the baseline and postresection ROI could be accurately aligned and the baseline tumor volume (N_t), residual tumor volume after resection ($N_{t'}$) and total volume of resected tumor (ΔN_t) could be calculated (Table 2). These results demonstrate that 56.5% of the tumor was resected with 43.5 % of residual tumor still present after tumor resection on the postresection images (Table 2).

Calculation of total grey and white matter resected

In 3 of 4 calf hemispheres with tumors the baseline grey (N_g) and white matter volume (N_w) within their respective ROI could be calculated (Table 2). In these 3 tumors, it was possible to calculate residual grey ($N_{g'}$) and residual white matter ($N_{w'}$) present in the ROI of the postresection images (Table 2). In brain hemisphere 4, the baseline and postresection images could not be accurately aligned since the resection cavity was compressed (Figure 5G and H). The ability to accurately calculate residual grey ($N_{g'}$) and residual white matter ($N_{w'}$) volumes present on the postresection images for 3 tumors allowed the for the calculation of change in grey (ΔN_g) and white matter volume (ΔN_w), resected grey and white matter respectively on the postresection images (Table 2). It was the expectation that more grey than white matter would be

removed during the subpial resection of tumors and the grey/white matter ratios appeared consistent with that expectation (Table 2).

Calculation of total tissue resected

For 2 tumors studied in which the tumor was completely removed ($\Delta N_t = 0$) and for the incompletely resected tumor, the total tumor resected volume (ΔN_t) was successfully calculated. Since it was also possible to calculate residual grey ($N_{g\prime}$), residual white matter ($N_{w\prime}$) and residual tumor (ΔN_t) volumes present on the postresection images the total volume of tissue removed (N_r) during the subpial resection could be calculated utilizing equation 7. The total tissue resected ranged from 0.524 to 7.337 mL (Table 2).

Postresection structural integrity analysis of grey and white matter tracks

The registration process of the baseline and postresection 7-Tesla MR images provided structural information on the integrity of grey matter gyri and white matter tracks in the vicinity of the tumor before and after tumor resection. By matching each point on the postresection segmented image with its analog on the baseline segmented image using the Slicer extension "Segmentation registration"[79], it was possible to evaluate the differences between both images after they were automatically registered by the software (Figure 5). On the baseline sagittal segmented images provided, the injected alginate resulted in irregular tumors within and covered by the overlying grey matter gyrus (Figure 5A, C, E, G). In some postresection segmented images, irregularities in the residual grey matter tissue can be visualized, which is consistent with incomplete resection of overlying grey matter and grey matter injury. (Figure 5F and 6D). Residual tumor tissue in this model can be identified and easily quantitated on postresection images (Figures 5 and 6). Although fiducials were only placed on 1 brain in Group 2, their presence improved baseline and postresection image alignment by acting as landmarks which could be easily recognized and

registered. A supplemental video containing scrolling coronal baseline and postresection images is provided for brain 1 Group 2 and brain 3 of Group 2. These videos can be used to provide the learner with further information on the surgical performance. Violation of the surgical pial boundaries and damage to the adjacent gyrus are particularly apparent when both baseline and postresection segmented MRIs are put side by side for comparison.

Baseline and postresection three-dimensional reconstruction views

Using the information available on the segmented baseline and postresection images, it is possible to develop three-dimensional (3D) reconstructions of the calf brain containing the tumor and postresection residual tumor (Figure 7). These images can provide further information related to the surface structure of the resection cavity and the 3D structure of the tumor within the calf brain both before and after resection; in the case of brain 1 of Group 2, this sort of 3D view allowed the visualization of the residual tumor remaining after the subtotal resection (Figure 7).

DISCUSSION

Summary

This pilot study was carried out as a proof of concept that the combination of utilizing a brain tumor resection model and segmented 7-Tesla MRIs is feasible and has the potential to aid in understanding and evaluating neurosurgical performance. We were able to fulfill our aims of quantitating brain tissue removal, alginate brain tumor resected, normal grey and white matter resected along with total tissue resected after subpial resection in a calf brain model.

Quantification of brain tissue removed

The image analysis based on segmented 7-Tesla MRIs utilized in this study can be used with the developed polynomial model to accurately predict small brain segment removals if brain

deformation between baseline and postresection images is minimal. Indeed, significant deformation of anatomical structures in the baseline and postresection images prevents the registration of the two images, thus preventing the calculation of the difference in tissue volumes between the two images. Another limiting factor is the size of the removed piece of tissue. Smaller pieces cannot be accurately analyzed as they can easily be mistaken for brain surface deformation. The polynomial model can determine the brain tissue weights in grams when larger amounts of brain are removed. Further investigation needs to be performed to increase our ability to measure smaller quantities of brain tissue removed.

Alginate tumor model and quantitative analysis of tissue resections

Although attempts were made to provide the ex-vivo alginate tumor model utilized with color and tumor stiffness characteristics associated with human tumors, the model does not reproduce the multiple consistencies and bleeding associated with human glial tumors. Therefore, our studies are not able to assess the influence of these factors of resection technique. The alginate tumor hydro-dissection injection into calf brain cortical grey matter resulted in a variety of tumor shapes necessitating careful delineation of the ROI on the baseline and postresection images (Figure 5). The alginate tumor model and the segmentation and registration 7-Tesla MRI techniques utilized in this study allowed quantitative assessment of all 4 tumor volumes (N_t) and 3 out of 4 grey matter (N_g) and white matter (N_w) volumes within ROI outlined on baseline scans. The quantitation of residual grey matter ($N_{g'}$), residual white matter ($N_{w'}$) along with the residual tumor ($N_{t'}$) in the equivalent ROI location after resection is important to allow calculation of change in grey matter (ΔN_g), change in white matter (ΔN_w) and change in tumor (ΔN_t). Using equation 7, the value for total resected tissue (N_r) can be obtained. This is only possible if accurate alignment of baseline and postresection images can be achieved and this was

accomplished in 3 of 4 tumors studied. Although only a small series, 4 of 7 calf hemispheres studied contained fiducials. There appeared to be an improvement in registration of baseline and postresection segmented images when fiducials were present. Accurate registration was not possible for the largest tumor in the series due to the infolding and collapse of the resection cavity during placement in the MRI coil (Figure 5). This suggested that larger resection cavities tend to be more compressible after being placed in the coil. Conceptually, filling the resection cavity after the completion of the procedure with an incompressible material that is not visible on MRI would result in lesser deformation, allow improved alignment and increase the ability to find all 3 variables necessary to solve equation 7. Studies are ongoing to evaluate possible materials which could perform this function.

Educational Opportunities: Combining Virtual Reality and ex-vivo models

Ex-vivo models have been developed to aid in the assessment of neurosurgical technical skills. The ex-vivo bovine model used in these studies is not an exact replicate for the human brain regarding size and convolutional surface appearance and should not be considered a substitute for the detailed anatomical studies involving cadaveric models. However, ex-vivo models do provide new methods to quantitate trainees' technical skills and different educational opportunities for learners. MR imaging has not been previous employed to assess psychomotor bimanual performance in these model systems. Pre and postresection imaging, whether MR or CT[80], is available on patients undergoing operation for tumor resection but the ability to accurately quantitate grey and white matter removal in these procedures is difficult. The ability to use this tumor model in combination with 7-Tesla MR imaging provides an opportunity to increase the granularity of data obtainable from operative procedures. Our group has utilized high fidelity virtual reality simulators with haptic feedback to develop a model for bimanual

psychomotor surgical performance[8] and for quantitative assessment of expert performance.[63, 81] Present studies are focused on developing intelligent tutoring systems using machine learning[73] and artificial neural networks[82] for assessment and training of surgical performance[83] along with the development of complex neurosurgical scenarios for use in these tutoring sytems.[84, 85] The ability to compare expert performance on surgical virtual reality simulators to that in controlled operating room environments would advance both the understanding of surgical expertise and the ability to train learners to the mastery level using these intelligent tutoring systems.[83, 86] The combination of developing standardized alginate tumor and epilepsy models utilizing the ex-vivo calf brain model outlined in this communication along with segmentation and registration MRI technologies allows for future studies in skills transfer between virtual reality simulators and the operating room. These investigations would be able to focus not only on amount of tumor tissue resected but quantity of normal grey matter and white matter tracts resected, the method of resection and the tissue injury to adjacent areas.

LIMITATIONS

Although this is to our knowledge the first study that attempts to provide a quantitative method of analysis on an artificial tumor model obtained from a 7-Tesla MRI scanner, there are limitations. First, the polynomial model developed using brain sections involving both grey and white matter was limited and needs to be expanded. Our polynomial model was based on 4 brain segments; further studies with different sizes of brain tissue removed must be carried to increase the accuracy and predictive power of the model. Second, to quantitate residual grey and white matter in the postresection segmented images, methods to prevent infolding of the resection cavity need to be developed to avoid being unable to register pre and postresection segmented MRIs such as in the case of brain 4 (Figure 5H). Studies are underway to address this issue.

Third, this model does not allow for an assessment of vascular injury but methods to perfuse the ex-vivo calf brain hemispheres are being explored. Fourth, regarding segmentation, although manual segmentation remains the gold standard, it induces a range of variability in accuracy which may affect the quality of the segmentations.[42, 45, 46] Variability may result from user factors and signal inhomogeneity of the volume despite the filtering process, particularly when same tissue types display residual noise.[87] Manual segmentation requires significantly higher amount of time compared to automatic methods, which may not be adapted to the clinical setting. Choosing the proper ROI after segmentation and registration is also time-consuming and requires expertise. For instance, the processing of brain 4 was not possible not only because the post-resection cavity collapsed on itself but also because only half of the brain was scanned, thus omitting important brain landmarks that could have been used to perform registration. The choice of FOV for this brain was done with the idea that scanning the half of the brain that contains the tumor would be easier than scanning the whole brain. No atlas or database on calf brain exists which makes the development of an automated segmentation pipeline difficult. The number of calf brain hemispheres used in this pilot study was small. However, these investigations functioned as a proof of concept and outlined important issues that need to be addressed to improve future studies. Only a small number of institutions have access to animal 7-Tesla MRI units limiting the number of research centers that can carry out these types of investigations. Studies utilizing human 7-Tesla MRI to quantitate operative performance may also find these studies useful.

CONCLUSION

This pilot study was carried out as a proof of concept to demonstrate the feasibility of using brain tumor models combined with 7-Tesla MR imaging technology to quantitate brain tumor

resection along with normal grey matter, normal white matter and total tissue resected after subpial resection procedures in a calf brain *ex-vivo* tumor model. The ability to use tumor models in combination with 7-Tesla MR imaging provides an opportunity to increase the granularity of data obtained from operative procedures and improve the assessment and training of learners.

ACKNOWLEDGEMENT

The authors would like to thank Dr. Carlo Santaguida, Department of Neurology and Neurosurgery, Montreal Neurological Institute and Hospital, McGill University for his help with this project.

FUNDING

This work was supported by the Franco Di Giovanni Foundation, the Montreal English School Board, the Montreal Neurological Institute and Hospital. Dr. Winkler-Schwartz received a Doctoral Training Grant for Applicants with a Professional Degree the Fonds de recherche du Québec – Santé (fund # 261422) and holds the Robert Maudsley Fellowship for Studies in Medical Education by the Royal College of Physicians and Surgeons of Canada.

DISCUSSION OF THESIS

Developing quantitative assessment methods for training bimanual psychomotor performance utilizing ex-vivo brain tumor models is important to establish these models as reliable platforms for the formative and summative assessment of surgical skills. Most studies describing these types of models use visual assessment of performance on these platforms by expert surgeons. The proposed method of segmentation and registration of 7-Tesla MR scans outlined in this study increases the objectivity and granularity of trainee surgical assessment. Although this study explored the use of 7-Tesla segmented MRIs to assess surgical performance immersive learning cannot be limited to the quality of the psychomotor skills of surgeons. Other parameters, such as teamwork abilities, intrinsic competencies and stress management also need to be included in a comprehensive learning curriculum.

Future directions

This study was a pilot study to assess the feasibility of using 7-Tesla MRIs to assess surgical performance using an ex-vivo brain tumor model. Although the methodology used here relies on manual segmentation of MRIs, segmentation and registration can be significantly shortened by developing a pipeline to process large quantities of MR scans in a relatively short period of time. Such automatic segmentation methods already exist in the field of human brain imaging, with statistical and probabilistic models for brain segmentation created using large quantities of brain image data[47-50]. These methods include atlas-based, model-based, region-based, amplitude and edge-based segmentations. Such platforms allow for regular formative assessment of surgical skills and self-guided learning. In addition, this system could help residents perform complex surgical techniques and targeted learning of specific psychomotor skills to improve their surgical performance.

An important step to develop our methodology further would be to create a brain atlas or probabilistic model of calf brains. To our knowledge, no such atlas currently exists for bovine brains. Technologies such as the NeuroVR simulator platform can be exploited in combination with ex-vivo brain tumor models to give surgical trainees the tools they need to fully develop their set of motor skills to the level of mastery. Since this was only a pilot study, the polynomial model proposed needs to be further developed utilizing data from further experiments.

THESIS CONCLUSION

This thesis outlined a quantitative and visual methodology to analyze surgical performance on the resection of alginate artificial tumors in an ex-vivo bovine calf model using 7-Tesla MR scans. The aims of this pilot study were to: 1) To determine if the assessment of baseline images and postresection images acquired using 7-Tesla MRI scanner can accurately quantitate normal brain tissue removed in a ex-vivo bovine calf brain model, 2) To assess if baseline and postresection 7-Tesla MR imaging technology can quantitate alginate brain tumor resected after subpial resection in a ex-vivo bovine calf brain model and 3) To outline if baseline and postresection 7-Tesla MR imaging technology can quantitate grey matter, white matter and total tissue resection following subtotal and total subpial resection of alginate brain tumor in a ex-vivo bovine calf brain model. The three aims of the study have been fulfilled. First, it was possible to quantitate from the 7T MR scans of calf brains the amount of normal tissue resected by comparing the differences between baseline and postresection segmented images. Second, this 7-Tesla MR imaging technology was able to quantitate alginate brain tumor resected after subpial resection in an ex-vivo bovine calf brain model. Third, this methodology quantitated grey matter, white matter and total tissue resection after subpial resection in an ex-vivo bovine calf brain model. This quantitative analysis was supplemented with visual analysis of the post-resection

brain images, allowing us to extract information on normal grey matter tissue injury and white matter tract removal.

This study suggests that an ex-vivo bovine calf brain tumor model can be objectively analyzed to provide surgical trainees and surgical educators with quantitative metrics to objectively assess surgical performance in safe controlled environment. The development of quantifiable surgical metrics for expert surgical performance will be useful to surgical educators in improving bimanual psychomotor operative performance.

REFERENCES

1. Stefanou MI. The footprints of neuroscience in Alexandria during the 3rd-century BC: Herophilus and Erasistratus. *J Med Biogr*. 2020;28(4): 186-194. https://doi.org/10.1177/0967772018789349.

2. Aggarwal A. The evolving relationship between surgery and medicine. *AMA Journal of Ethics*. 2010;12(2): 119-123.

3. Ghosh SK. Human cadaveric dissection: a historical account from ancient Greece to the modern era. *Anat Cell Biol*. 2015;48(3): 153-169. https://doi.org/10.5115/acb.2015.48.3.153.

4. Ackerknecht EH. From barber-surgeon to modern doctor. *Bull Hist Med*. 1984;58(4): 545-553.

5. Kaya Y, Sindel A. John Hunter (1728-1793) and his legacy to science. *Childs Nerv Syst*. 2016;32(6): 1015-1017. https://doi.org/10.1007/s00381-015-2852-x.

6. Osborne MP. William Stewart Halsted: his life and contributions to surgery. *Lancet Oncol*. 2007;8(3): 256-265. https://doi.org/10.1016/S1470-2045(07)70076-1.

7. Sealy WC. Halsted is dead: Time for change in graduate surgical education. *Curr Surg*. 1999;56(1-2): 34-39. https://doi.org/10.1016/s0149-7944(99)00005-7.

8. Wilde S, Hirst G. Learning from mistakes: early twentieth-century surgical practice. *J Hist Med Allied Sci*. 2009;64(1): 38-77. https://doi.org/10.1093/jhmas/jrn055.

9. Elmore LC, Jeffe DB, Jin L, Awad MM, Turnbull IR. National Survey of Burnout among US General Surgery Residents. *J Am Coll Surg*. 2016;223(3): 440-451. https://doi.org/10.1016/j.jamcollsurg.2016.05.014.

10. Jarman BT, Miller MR, Brown RS, et al. The 80-hour work week: will we have less-experienced graduating surgeons? *Curr Surg.* 2004;61(6): 612-615. https://doi.org/10.1016/j.cursur.2004.06.016.

11. Gelinas-Phaneuf N, Del Maestro RF. Surgical expertise in neurosurgery: integrating theory into practice. *Neurosurg.* 2013;73 Suppl 1: 30-38. https://doi.org/10.1227/NEU.0000000000000115.

12. Thiels CA, Choudhry AJ, Ray-Zack MD, et al. Medical Malpractice Lawsuits Involving Surgical Residents. *JAMA Surg.* 2018;153(1): 8-13. https://doi.org/10.1001/jamasurg.2017.2979.

13. Kessler RA, Benzil DL, Loewenstern J, et al. Malpractice Litigation in Brain Tumor Surgery: A 31-Year Analysis of Causative Factors in the United States from the Westlaw Database. *World Neurosurg.* 2019;122: e1570-e1577. https://doi.org/10.1016/j.wneu.2018.11.112.

14. Jena AB, Seabury S, Lakdawalla D, Chandra A. Malpractice risk according to physician specialty. *N Engl J Med.* 2011;365(7): 629-636. https://doi.org/10.1056/NEJMsa1012370.

15. Balch CM, Oreskovich MR, Dyrbye LN, et al. Personal consequences of malpractice lawsuits on American surgeons. *J Am Coll Surg.* 2011;213(5): 657-667. https://doi.org/10.1016/j.jamcollsurg.2011.08.005.

16. Choudhury N, Gélinas-Phaneuf N, Delorme S, Del Maestro R. Fundamentals of Neurosurgery: Virtual Reality Tasks for Training and Evaluation of Technical Skills. *World Neurosurg.* 2013;80(5): e9-e19. https://doi.org/10.1016/j.wneu.2012.08.022.

17. Ashour AM, Elbabaa SK, Caputy AJ, Gragnaniello C. Navigation-Guided Endoscopic Intraventricular Injectable Tumor Model: Cadaveric Tumor Resection Model for Neurosurgical Training. *World Neurosurg.* 2016;96: 261-266. https://doi.org/10.1016/j.wneu.2016.04.048.

18. Aurich LA, Silva Junior LF, Monteiro FM, Ottoni AN, Jung GS, Ramina R. Microsurgical training model with nonliving swine head. Alternative for neurosurgical education. *Acta Cir Bras.* 2014;29(6): 405-409. https://doi.org/10.1590/s0102-86502014000600010.

19. Berhouma M, Baidya NB, Ismail AA, Zhang J, Ammirati M. Shortening the learning curve in endoscopic endonasal skull base surgery: a reproducible polymer tumor model for the trans-sphenoidal trans-tubercular approach to retro-infundibular tumors. *Clin Neurol Neurosurg.* 2013;115(9): 1635-1641. https://doi.org/10.1016/j.clineuro.2013.02.013.

20. Csokay A, Papp A, Imreh D, Czabajszky M, Valalik I, Antalfi B. Modelling pathology from autolog fresh cadaver organs as a novel concept in neurosurgical training. *Acta Neurochir (Wien).* 2013;155(10): 1993-1995. https://doi.org/10.1007/s00701-013-1727-8.

21. Gragnaniello C, Gagliardi F, Chau AM, et al. Intracranial injectable tumor model: technical advancements. *J Neurol Surg B Skull Base.* 2014;75(5): 301-308. https://doi.org/10.1055/s-0034-1368148.

22. Kamp MA, Knipps J, Steiger HJ, et al. Training for brain tumour resection: a realistic model with easy accessibility. *Acta Neurochir (Wien).* 2015;157(11): 1975-1981; discussion 1981. https://doi.org/10.1007/s00701-015-2590-6.

23. Mashiko T, Oguma H, Konno T, et al. Training of Intra-Axial Brain Tumor Resection Using a Self-Made Simple Device with Agar and Gelatin. *World Neurosurg.* 2018;109: e298-e304. https://doi.org/10.1016/j.wneu.2017.09.162.

24. Tan SS, Sarker SK. Simulation in surgery: a review. *Scott Med J.* 2011;56(2): 104-109. https://doi.org/10.1258/smj.2011.011098.

25. Rehder R, Abd-El-Barr M, Hooten K, Weinstock P, Madsen JR, Cohen AR. The role of simulation in neurosurgery. *Childs Nerv Syst.* 2016;32(1): 43-54. https://doi.org/10.1007/s00381-015-2923-z.

26. Turan Suslu H, Ceylan D, Tatarli N, et al. Laboratory training in the retrosigmoid approach using cadaveric silicone injected cow brain. *Br J Neurosurg.* 2013;27(6): 812-814. https://doi.org/10.3109/02688697.2013.772095.

27. Valli D, Belykh E, Zhao X, et al. Development of a Simulation Model for Fluorescence-Guided Brain Tumor Surgery. *Front Oncol.* 2019;9: 748. https://doi.org/10.3389/fonc.2019.00748.

28. Kneebone R. Simulation in surgical training: educational issues and practical implications. *Med Educ.* 2003;37(3): 267-277. https://doi.org/10.1046/j.1365-2923.2003.01440.x.

29. Gélinas-Phaneuf N, Choudhury N, Al-Habib AR, et al. Assessing performance in brain tumor resection using a novel virtual reality simulator. *Int J Comput Assist Radiol Surg.* 2013;9(1): 1-9. https://doi.org/10.1007/s11548-013-0905-8.

30. Delorme S, Laroche D, DiRaddo R, Del Maestro RF. NeuroTouch: a physics-based virtual simulator for cranial microneurosurgery training. *Neurosurg.* 2012;71(1 Suppl Operative): 32-42. https://doi.org/10.1227/NEU.0b013e318249c744.

31. Silbergeld D, Hebb A, Yang T. The sub-pial resection technique for intrinsic tumor surgery. *Surg Neurol Int.* 2011;2(1): 180-180. https://doi.org/10.4103/2152-7806.90714.

32. Hervey-Jumper SL, Berger MS. Role of surgical resection in low- and high-grade gliomas. *Curr Treat Options Neurol.* 2014;16(4): 284. https://doi.org/10.1007/s11940-014-0284-7.

33. Tomlinson SB, Hendricks BK, Cohen-Gadol AA. Editorial. Innovations in neurosurgical education during the COVID-19 pandemic: is it time to reexamine our neurosurgical training models? *J Neurosurg.* 2020;133(1): 14-15. https://doi.org/10.3171/2020.4.Jns201012.

34. Winkler-Schwartz A, Yilmaz R, Tran DH, et al. Creating a Comprehensive Research Platform for Surgical Technique and Operative Outcome in Primary Brain Tumor Neurosurgery. *World Neurosurg.* 2020. https://doi.org/10.1016/j.wneu.2020.07.209.

35. Morosanu CO, Nicolae L, Moldovan R, Farcasanu AS, Filip GA, Florian IS. Neurosurgical cadaveric and in vivo large animal training models for cranial and spinal approaches and techniques — a systematic review of the current literature. *Neurol Neurochir Pol.* 2018;53(1): 8-17. https://doi.org/10.5603/PJNNS.a2019.0001.

36. Berger A. Magnetic resonance imaging. *BMJ.* 2002;324(7328): 35. https://doi.org/10.1136/bmj.324.7328.35.

37. Grover VP, Tognarelli JM, Crossey MM, Cox IJ, Taylor-Robinson SD, McPhail MJ. Magnetic Resonance Imaging: Principles and Techniques: Lessons for Clinicians. *J Clin Exp Hepatol.* 2015;5(3): 246-255. https://doi.org/10.1016/j.jceh.2015.08.001.

38. Miloushev VZ, Keshari KR, Holodny AI. Hyperpolarization MRI. *Top Magn Reson Imaging.* 2016;25(1): 31-37. https://doi.org/10.1097/rmr.0000000000000076.

39. Ross BD, Bhattacharya P, Wagner S, Tran T, Sailasuta N. Hyperpolarized MR Imaging: Neurologic Applications of Hyperpolarized Metabolism. *Am J Neuroradiol.* 2010;31(1): 24-33. https://doi.org/10.3174/ajnr.A1790.

40. Ladd ME, Bachert P, Meyerspeer M, et al. Pros and cons of ultra-high-field MRI/MRS for human application. *Prog Nucl Magn Reson Spectrosc.* 2018;109: 1-50. https://doi.org/10.1016/j.pnmrs.2018.06.001.

41. Rutt BK, Lee DH. The impact of field strength on image quality in MRI. *J Magn Reson Imaging.* 1996;6(1): 57-62. https://doi.org/10.1002/jmri.1880060111.

42. Despotović I, Goossens B, Philips W. MRI Segmentation of the Human Brain: Challenges, Methods, and Applications. *Comput Math Methods Med.* 2015;2015: 1-23. https://doi.org/10.1155/2015/450341.

43. Loizou CP, Papacharalambous C, Samaras G, et al. Brain Image and Lesions Registration and 3D Reconstruction in Dicom MRI Images. *2017 IEEE 30th International Symposium on Computer-Based Medical Systems (CBMS).* 2017:419-422.

44. Roy S, Bandyopadhyay SK. Detection and Quantification of Brain Tumor from MRI of Brain and it's Symmetric Analysis. *Int J Inf Commun Technol.* 2012;2(6).

45. Abdallah MB, Blonski M, Wantz-Mézières S, Gaudeau Y, Taillandier L, Moureaux J-M. Statistical evaluation of manual segmentation of a diffuse low-grade glioma MRI dataset. *2016 38th Annual International Conference of the IEEE Engineering in Medicine and Biology Society (EMBC).* IEEE; 2016:4403-4406.

46. Veeraraghavan H, Miller JV. Active learning guided interactions for consistent image segmentation with reduced user interactions. *2011 IEEE International Symposium on Biomedical Imaging: From Nano to Macro.* 2011:1645-1648.

47. Coupe P, Manjon JV, Fonov V, Pruessner J, Robles M, Collins DL. Patch-based segmentation using expert priors: application to hippocampus and ventricle segmentation. *Neuroimage.* 2011;54(2): 940-954. https://doi.org/10.1016/j.neuroimage.2010.09.018.

48. Mechrez R, Goldberger J, Greenspan H. Patch-Based Segmentation with Spatial Consistency: Application to MS Lesions in Brain MRI. *Int J Biomed Imaging.* 2016;2016: 1-13. https://doi.org/10.1155/2016/7952541.

49. Fischl B, Salat DH, Busa E, et al. Whole Brain Segmentation. *Neuron.* 2002;33(3): 341-355. https://doi.org/10.1016/s0896-6273(02)00569-x.

50. Sharma N, Aggarwal LM. Automated medical image segmentation techniques. *J Med Phys.* 2010;35(1): 3-14. https://doi.org/10.4103/0971-6203.58777.

51. Zhang Z, Cho S, Rehni AK, Quero HN, Dave KR, Zhao W. Automated Assessment of Hematoma Volume of Rodents Subjected to Experimental Intracerebral Hemorrhagic Stroke by Bayes Segmentation Approach. *Transl Stroke Res.* 2020;11(4): 789-798. https://doi.org/10.1007/s12975-019-00754-3.

52. de Brebisson A, Montana G. Deep neural networks for anatomical brain segmentation. *Proceedings of the IEEE Conference on Computer Vision and Pattern Recognition Workshops.* 2015:20-28.

53. Pichon E, Tannenbaum A, Kikinis R. A statistically based flow for image segmentation. *Med Image Anal.* 2004;8(3): 267-274. https://doi.org/10.1016/j.media.2004.06.006.

54. Kim YJ, Lee SH, Park CM, Kim KG. Evaluation of Semi-automatic Segmentation Methods for Persistent Ground Glass Nodules on Thin-Section CT Scans. *Healthc Inform Res.* 2016;22(4): 305-315. https://doi.org/10.4258/hir.2016.22.4.305.

55. Tingelhoff K, Moral AI, Kunkel ME, et al. Comparison between Manual and Semi-automatic Segmentation of Nasal Cavity and Paranasal Sinuses from CT Images. *2007 29th Annual International Conference of the IEEE Engineering in Medicine and Biology Society.* 2007:5505-5508.

56. Otsu N. A Threshold Selection Method from Gray-Level Histograms. *IEEE Transactions on Systems, Man, and Cybernetics.* 1979;9(1): 62-66. https://doi.org/10.1109/tsmc.1979.4310076.

57. Adams R, Bischof L. Seeded region growing. *IEEE Trans Pattern Anal Mach Intell.* 1994;16(6): 641-647.

58. Holz D, Behnke S. Fast range image segmentation and smoothing using approximate surface reconstruction and region growing. *Intelligent autonomous systems 12.* Springer; 2013:61-73.

59. Mani VRS, rivazhagan DS. Survey of Medical Image Registration. *J Med Eng Technol.* 2013;1(2): 8-25.

60. Collins DL, Evans AC. Animal: Validation and Applications of Nonlinear Registration-Based Segmentation. *Intern J Pattern Recognit Artif Intell.* 2011;11(08): 1271-1294. https://doi.org/10.1142/s0218001497000597.

61. Pallud J, Taillandier L, Capelle L, et al. Quantitative morphological magnetic resonance imaging follow-up of low-grade glioma: a plea for systematic measurement of growth rates. *Neurosurg.* 2012;71(3): 729-739; discussion 739-740. https://doi.org/10.1227/NEU.0b013e31826213de.

62. Brightwell A, Grant J. Competency-based training: who benefits? *Postgrad Med J.* 2013;89(1048): 107-110. https://doi.org/10.1136/postgradmedj-2012-130881.

63. Azarnoush H, Alzhrani G, Winkler-Schwartz A, et al. Neurosurgical virtual reality simulation metrics to assess psychomotor skills during brain tumor resection. *Int J Comput Assist Radiol Surg.* 2014;10(5): 603-618. https://doi.org/10.1007/s11548-014-1091-z.

64. Azarnoush H, Siar S, Sawaya R, et al. The force pyramid: a spatial analysis of force application during virtual reality brain tumor resection. *J Neurosurg.* 2017;127(1): 171-181. https://doi.org/10.3171/2016.7.JNS16322.

65. Bugdadi A, Sawaya R, Olwi D, et al. Automaticity of Force Application During Simulated Brain Tumor Resection: Testing the Fitts and Posner Model. *J Surg Educ.* 2018;75(1): 104-115. https://doi.org/10.1016/j.jsurg.2017.06.018.

66. Sawaya R, Alsideiri G, Bugdadi A, et al. Development of a performance model for virtual reality tumor resections. *J Neurosurg.* 2019;131(1): 192-200. https://doi.org/10.3171/2018.2.Jns172327.

67. Sawaya R, Bugdadi A, Azarnoush H, et al. Virtual Reality Tumor Resection: The Force Pyramid Approach. *Oper Neurosurg (Hagerstown).* 2018;14(6): 686-696. https://doi.org/10.1093/ons/opx189.

68. Winkler-Schwartz A, Bajunaid K, Mullah MAS, et al. Bimanual Psychomotor Performance in Neurosurgical Resident Applicants Assessed Using NeuroTouch, a Virtual Reality Simulator. *J Surg Educ.* 2016;73(6): 942-953. https://doi.org/10.1016/j.jsurg.2016.04.013.

69. Jensen Ang WJ, Hopkins ME, Partridge R, et al. Validating the Use of Smartphone-Based Accelerometers for Performance Assessment in a Simulated Neurosurgical Task. *Oper Neurosurg.* 2014;10(1): 57-65. https://doi.org/10.1227/neu.0000000000000010.

70. Alotaibi FE, AlZhrani GA, Mullah MA, et al. Assessing Bimanual Performance in Brain Tumor Resection With NeuroTouch, a Virtual Reality Simulator. *Oper Neurosurg.* 2015;11(1): 89-98. https://doi.org/10.1227/neu.0000000000000631.

71. Holloway T, Lorsch ZS, Chary MA, et al. Operator experience determines performance in a simulated computer-based brain tumor resection task. *Int J Comput Assist Radiol Surg.* 2015;10(11): 1853-1862. https://doi.org/10.1007/s11548-015-1160-y.

72. Bajunaid K, Mullah MA, Winkler-Schwartz A, et al. Impact of acute stress on psychomotor bimanual performance during a simulated tumor resection task. *J Neurosurg.* 2017;126(1): 71-80. https://doi.org/10.3171/2015.5.JNS15558.

73. Winkler-Schwartz A, Yilmaz R, Mirchi N, et al. Machine Learning Identification of Surgical and Operative Factors Associated With Surgical Expertise in Virtual Reality Simulation. *JAMA Network Open.* 2019;2(8): e198363-e198363. https://doi.org/10.1001/jamanetworkopen.2019.8363.

74. Springer E, Dymerska B, Cardoso PL, et al. Comparison of Routine Brain Imaging at 3 T and 7 T. *Invest Radiol.* 2016;51(8): 469-482. https://doi.org/10.1097/rli.0000000000000256.

75. Trattnig S, Springer E, Bogner W, et al. Key clinical benefits of neuroimaging at 7 T. *NeuroImage.* 2018;168: 477-489. https://doi.org/10.1016/j.neuroimage.2016.11.031.

76. Fedorov A, Beichel R, Kalpathy-Cramer J, et al. 3D Slicer as an image computing platform for the Quantitative Imaging Network. *Magn Reson Imaging.* 2012;30(9): 1323-1341. https://doi.org/10.1016/j.mri.2012.05.001.

77. Tustison N, Gee J. N4ITK: Nick's N3 ITK implementation for MRI bias field correction. *Insight J.* 2009: 1-8.

78. Tustison NJ, Avants BB, Cook PA, et al. N4ITK: improved N3 bias correction. *IEEE Trans Med Imaging.* 2010;29(6): 1310-1320. https://doi.org/10.1109/TMI.2010.2046908.

79. Fedorov A, Khallaghi S, Sánchez CA, et al. Open-source image registration for MRI–TRUS fusion-guided prostate interventions. *Int J Comput Assist Radiol Surg.* 2015;10(6): 925-934. https://doi.org/10.1007/s11548-015-1180-7.

80. Grosch AS, Schroder T, Schroder T, Onken J, Picht T. Development and initial evaluation of a novel simulation model for comprehensive brain tumor surgery training. *Acta Neurochir (Wien).* 2020;162(8): 1957-1965. https://doi.org/10.1007/s00701-020-04359-w.

81. Alotaibi FE, AlZhrani GA, Sabbagh AJ, Azarnoush H, Winkler-Schwartz A, Del Maestro RF. Neurosurgical Assessment of Metrics Including Judgment and Dexterity Using the Virtual Reality Simulator NeuroTouch (NAJD Metrics). *Surg Innov.* 2015;22(6): 636-642. https://doi.org/10.1177/1553350615579729.

82. Mirchi N, Bissonnette V, Ledwos N, et al. Artificial Neural Networks to Assess Virtual Reality Anterior Cervical Discectomy Performance. *Oper Neurosurg (Hagerstown).* 2020;19(1): 65-75. https://doi.org/10.1093/ons/opz359.

83. Mirchi N, Bissonnette V, Yilmaz R, Ledwos N, Winkler-Schwartz A, Del Maestro RF. The Virtual Operative Assistant: An explainable artificial intelligence tool for simulation-based training in surgery and medicine. *PLoS One.* 2020;15(2): e0229596. https://doi.org/10.1371/journal.pone.0229596.

84. Sabbagh AJ, Bajunaid KM, Alarifi N, et al. Roadmap for Developing Complex Virtual Reality Simulation Scenarios: Subpial Neurosurgical Tumor Resection Model. *World Neurosurg.* 2020;139: e220-e229. https://doi.org/10.1016/j.wneu.2020.03.187.

85. Ledwos N, Mirchi N, Bissonnette V, Winkler-Schwartz A, Yilmaz R, Del Maestro RF. Virtual Reality Anterior Cervical Discectomy and Fusion Simulation on the Novel Sim-Ortho Platform: Validation Studies. *Oper Neurosurg (Hagerstown).* 2020. https://doi.org/10.1093/ons/opaa269.

86. Mirchi N, Ledwos N, Del Maestro RF. Intelligent Tutoring Systems: Re-Envisioning Surgical Education in Response to COVID-19. *Can J Neurol Sci.* 2020: 1-3. https://doi.org/10.1017/cjn.2020.202.

87. Withey DJ, Koles ZJ. Medical Image Segmentation: Methods and Software. *2007 Joint Meeting of the 6th International Symposium on Noninvasive Functional Source Imaging of the Brain and Heart and the International Conference on Functional Biomedical Imaging.* 2007:140-143.

APPENDIX

TABLES

Table 1: Removed brain tissue weights (gm) of 6 segments from 3 calf brain hemispheres.

Volumes derived from analysis of segmented images (mL) and predicted weights (gm) along with percent error were computed based on the polynomial model *p(x)* as detailed in Figure 3.

Segments	**1**	**2**	**3**	**4**	**5**	**6**
Recorded weight (gm)	0.17	0.27	0.54	0.66	0.86	1.9
Volume (mL)	___	0.214	___	0.696	0.821	1.963
Predicted weight (gm)	___	0.258	___	0.710	0.827	1.898
Percent error $\left(\left\lvert\frac{predicted-actual}{actual}\right\rvert \times 100\%\right)$	___	4.44%	___	7.58%	3.84%	0.11%

Table 2: Injected alginate tumor volumes (mL) and grey matter, white matter and tumor volumes (mL) in region of interest (ROI) from 4 calf brain hemispheres.

Volumes in mL were derived from segmented baseline and postresection images. The baseline ROI volume in mL was composed of grey matter (N_g), white matter (Nw) and tumor (Nt). The postresection ROI volume was composed of residual grey matter ($N_{g'}$), residual white matter (N_w'), residual tumor (Nt') and total resected tissue (N_r). The change in grey matter (ΔN_g), in white matter (ΔN_w) and in tumor (ΔN_t) volumes in mL were calculated between baseline and postresection segmented ROI images. Adding these values allowed the calculation of total resected tissue (N_r). Percentage tumor resected and residual tumor volumes, tumor lengths and total grey to total white matter ratios were also calculated. Percentage tumor resected and residual tumor volumes were calculated based on the volume of injected alginate tumor inferred from 7-Tesla MRIs.

Calf brain hemisphere	**Brain 1**	**Brain 2**	**Brain 3**	**Brain 4**
Volume of injected alginate tumor (mL)	0.5	0.5	1.0	1.5
Volume of alginate tumor N_t inferred from 7-Tesla MRIs (mL)	0.421	0.838	0.902	1.428
Tumor length (mm)	17.850	15.800	23.300	24.750
Baseline grey matter within ROI N_g (mL)	14.634	18.535	25.300	___
Baseline white matter within ROI N_w (mL)	7.848	6.037	14.049	___
Baseline ROI volume (mL)	22.903	25.410	40.251	___

Postresection tumor volume $N_{t'}$ (mL)	0.183	0	0	0
Resected tumor volume ΔN_t (mL)	0.238	0.838	0.902	1.428
Resected tumor volume (%)	56.5	100	100	100
Residual tumor volume (%)	43.5	0	0	0
Resected grey matter volume ΔN_g (mL)	0.145	1.968	5.901	___
Resected white matter volume ΔN_w (mL)	0.141	0.478	0.534	___
Ratio of grey matter resected to white matter resected	1.03:1	4.12:1	11.05:1	___
Total resected tissue volume N_r (mL)	0.524	3.284	7.337	___

FIGURES

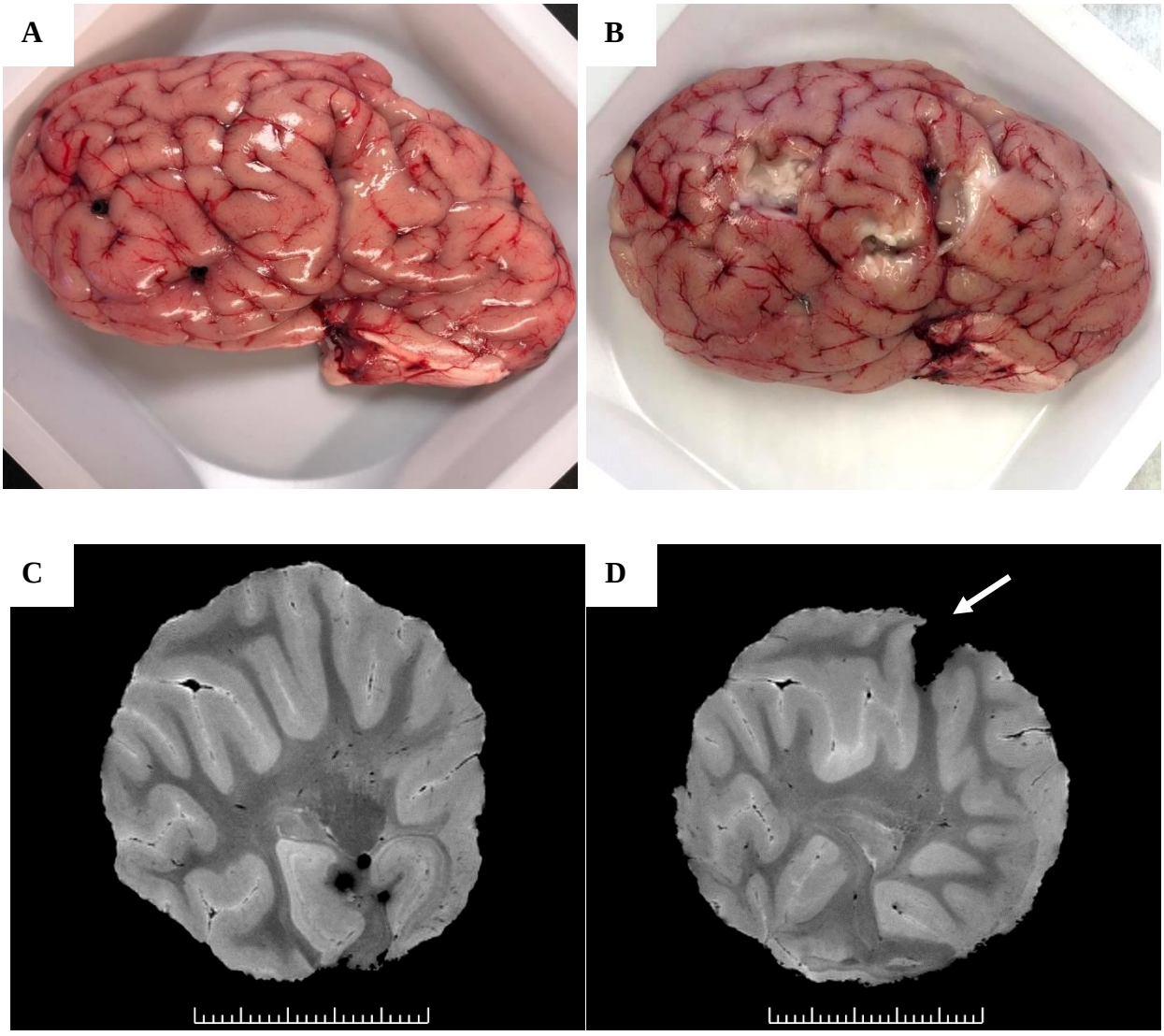

Figure 1: Calf brain from Group 1.

(A) Before resection of brain segments. (B) After resection of brain segments. (C) Coronal 7-Tesla MRI before segment resection (scale bar, 25mm). (D) Coronal 7-Tesla MRI after resection demonstrating area (arrow) of brain segment removed (scale bar, 25mm).

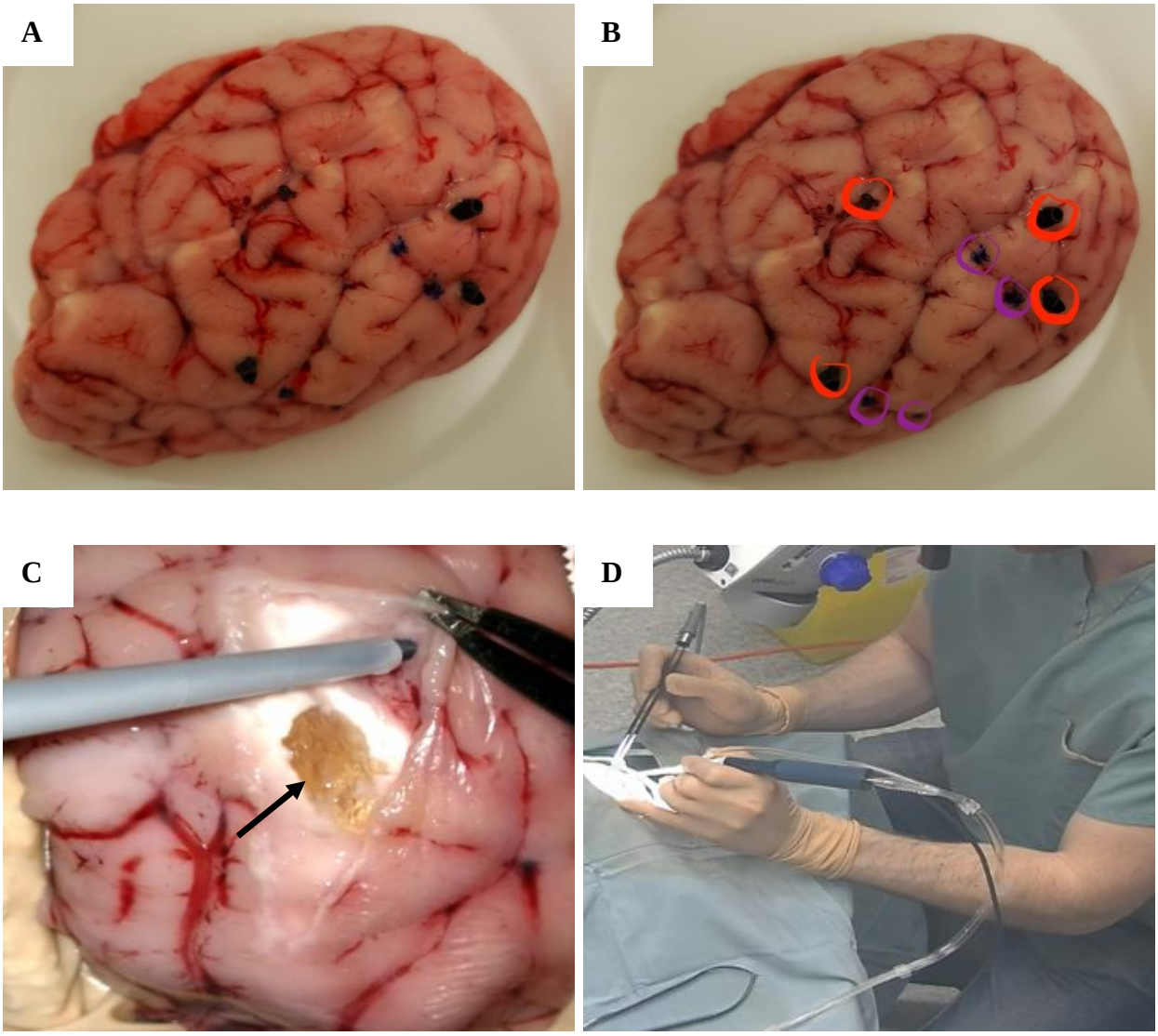

Figure 2: Calf brain hemisphere from Group 2.

(A) Inserted fiducials and markings outlining gyrus containing alginate tumor**.** (B) Fiducials are outlined in red and the gyrus to be resected containing tumor is between the marking outlined in blue. (C) View through the operating microscope demonstrating the bipolar forceps holding the pia and ultrasonic aspirator being used to carry out a subpial gyral resection involving the grey matter overlying the visualized tumor (arrow). (D) Operator carrying out the subpial gyral resection and the tumor resection.

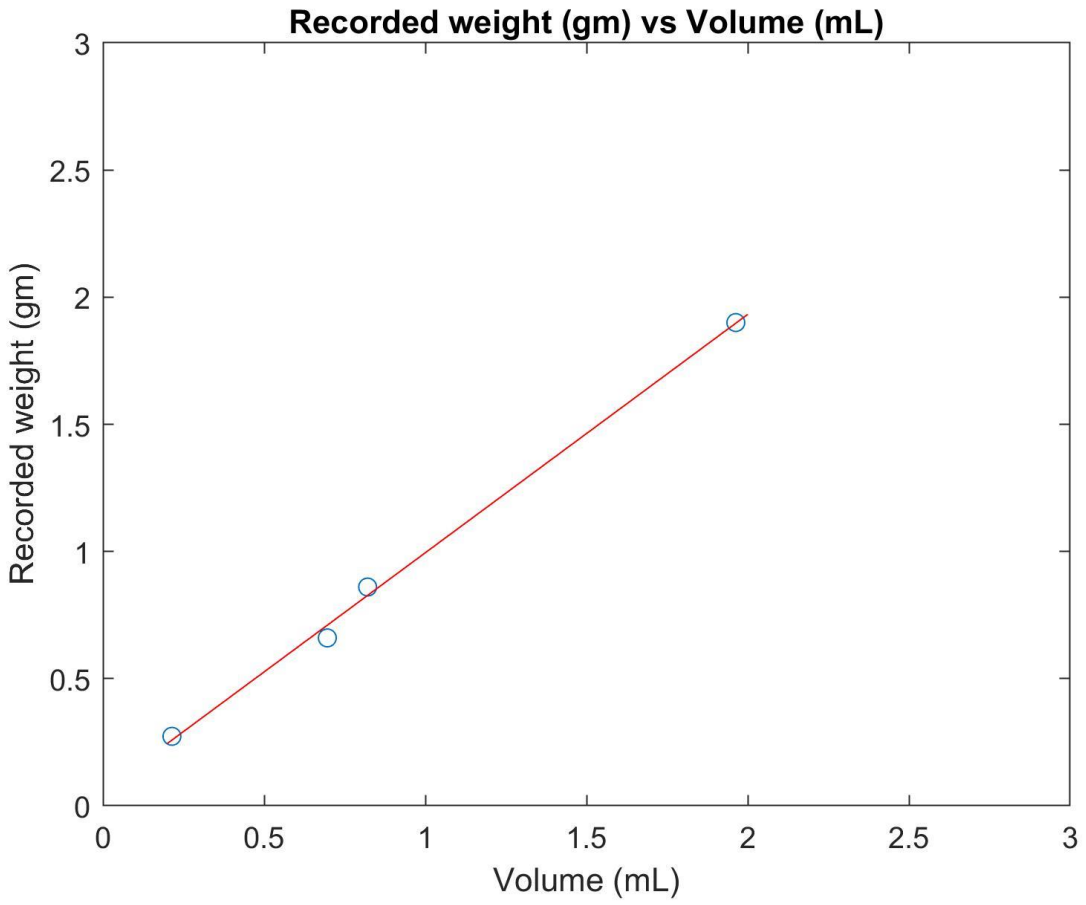

Figure 3: Recorded weights (gm) of resected brain segments versus their associated volumes (mL) determined from segmented images.

Data points shown here are listed in Table 1. To illustrate this quasi-linearity, a polynomial $p(x) = 0.9373\,x + 0.0576$ was fitted and plotted. A correlation coefficient of 0.9987 and an R^2 of 0.9974 between recorded weights and predicted weights have been found, suggesting good correlation between the two measures.

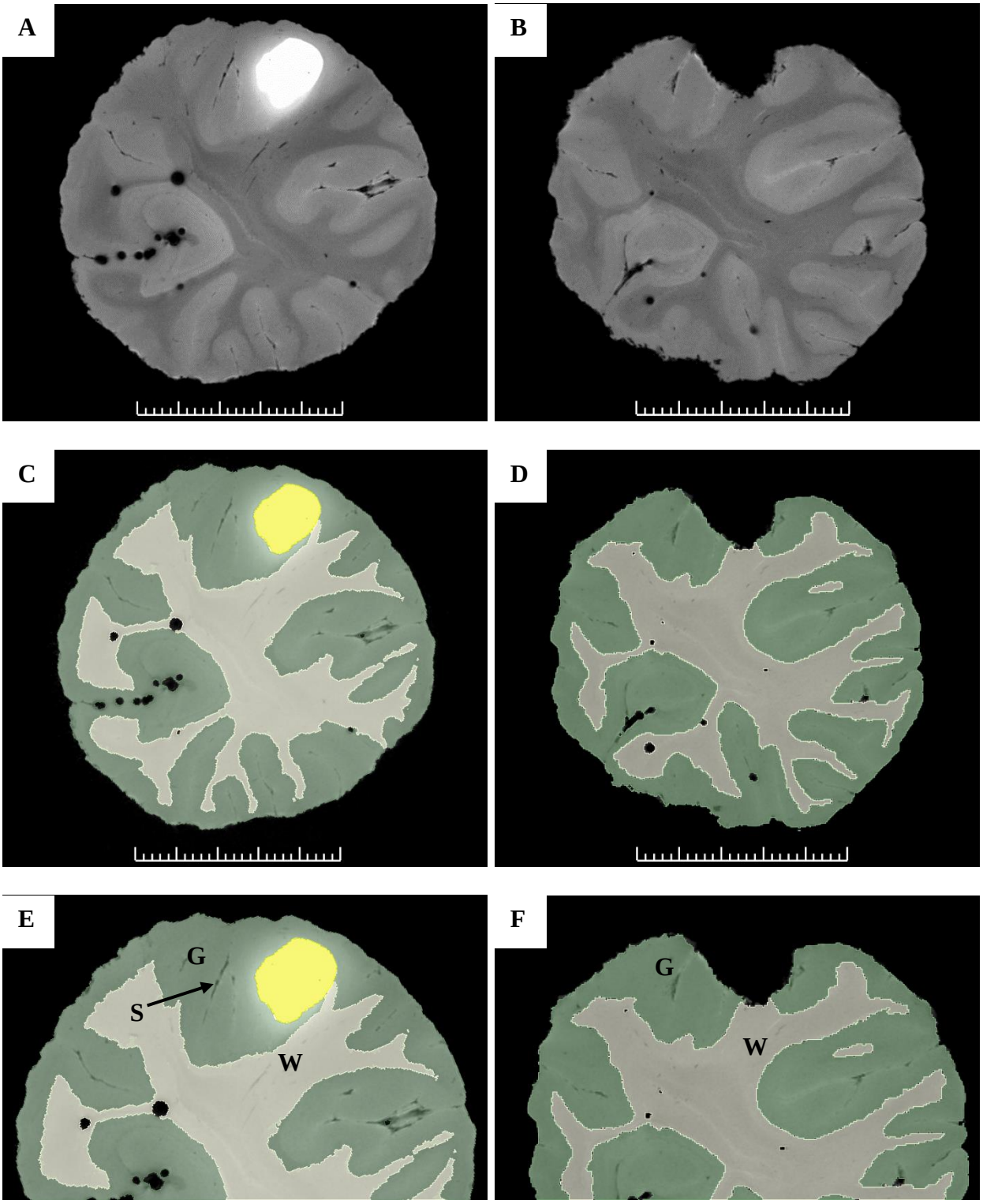
A
B
C
D
E
G
S
W
F
G
W

Figure 4: Coronal 7-Tesla MRIs of calf brain hemisphere containing alginate tumor (Group 2, calf brain hemisphere 2).

(A) Baseline enhancing tumor (scale bar, 25mm). (B) Postresection image after subpial gyral and tumor resection (scale bar, 25mm). (C). Baseline segmented image of enhancing tumor (scale bar, 25mm). (D) Postresection segmented image after subpial gyral and tumor resection (scale bar, 25mm). (E) Detailed view of baseline enhancing tumor with compressed grey matter gyrus G, displaced gyral sulcus S (arrow) and white matter W. (F) Detailed view of segmented image after subpial resection of overlying gyrus and tumor resection, demonstrating the re-expanded intact adjacent grey matter gyrus with sulcus along with resection of white matter.

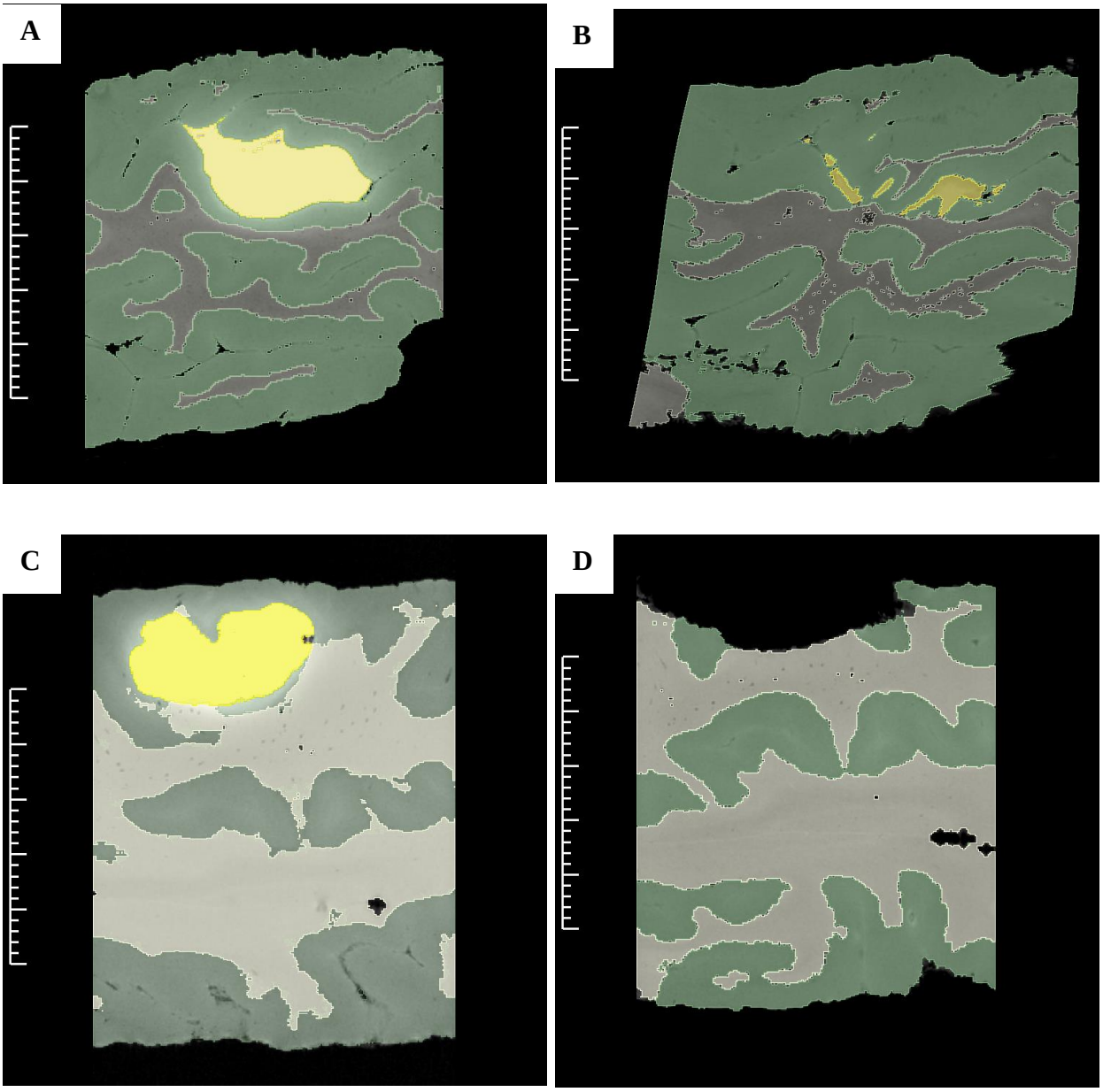
A
B
C
D

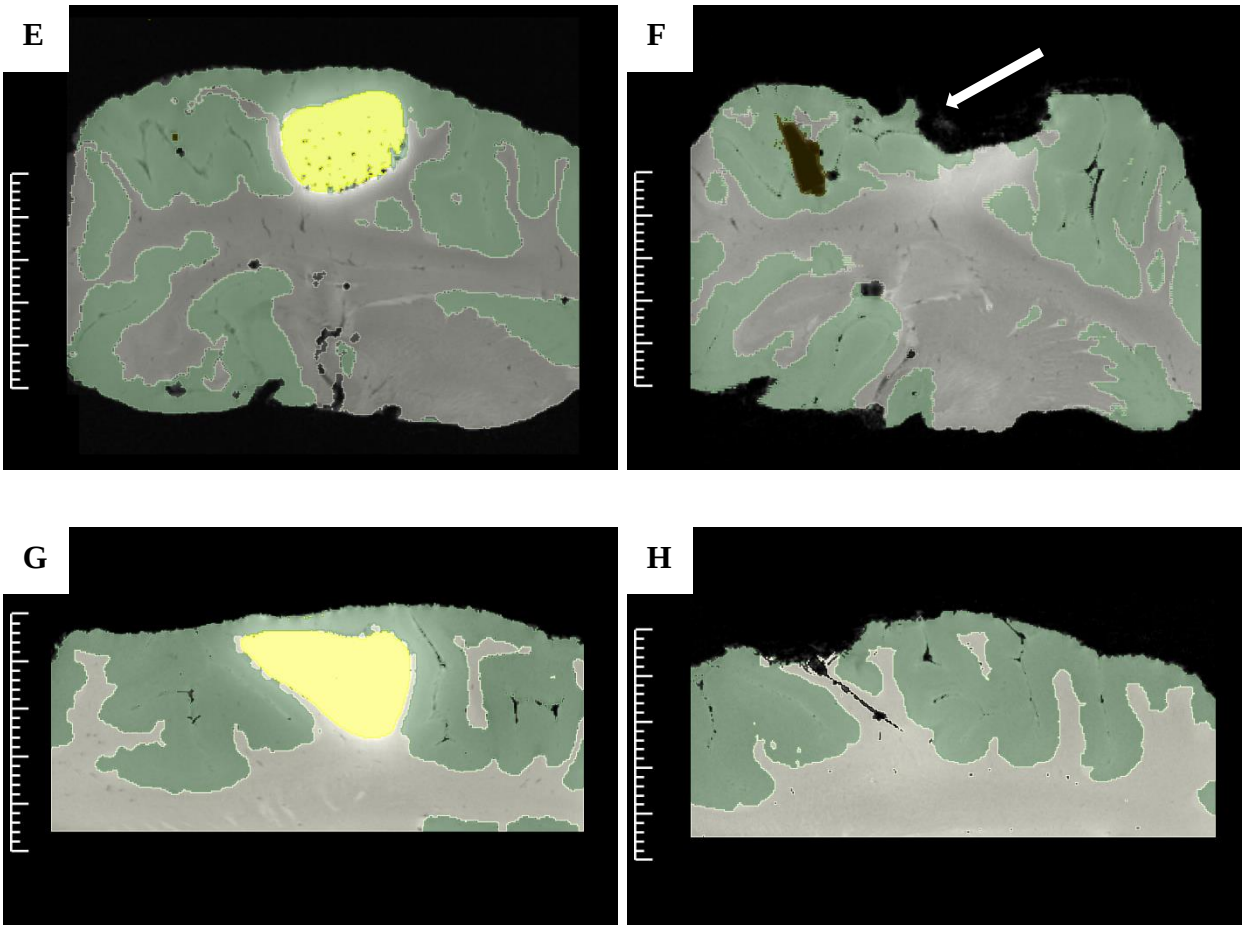

Figure 5: Sagittal 7-Tesla MRIs of calf brain hemisphere containing alginate tumors, Group 2.

(A) Baseline segmented sagittal image of irregular tumor in calf brain hemisphere 1 (scale bar, 25mm). (B) Postresection segmented sagittal image of brain hemisphere 1 after subpial gyral and tumor resection, demonstrating subtotal resection with residual tumor (scale bar, 25mm). (C) Baseline segmented sagittal image of tumor in calf brain hemisphere 2 demonstrating an elongated irregular tumor (scale bar, 25mm). (D) Postresection segmented sagittal image of brain hemisphere 2 after subpial gyral and tumor resection, demonstrating resection of overlying gyral grey matter along with complete tumor resection (scale bar, 25mm). (E) Baseline segmented sagittal image of tumor in calf brain hemisphere 3, demonstrating an oval shaped tumor (scale

bar, 25mm). (F) Postresection segmented sagittal image of brain hemisphere 3 after subpial gyral and tumor resection, demonstrating resection of overlying gyral grey matter and white matter tract. Residual regions of grey matter tissue irregularities in the resection cavity (arrow) consistent with residual grey matter and grey matter injury are also apparent (scale bar, 25mm). (G) Baseline segmented sagittal image of tumor in calf brain hemisphere 4 demonstrating the presence of tumor in the white matter (scale bar, 25mm). (H) Postresection segmented sagittal image of brain hemisphere 4 after subpial gyral and tumor resection demonstrating collapse of the resection cavity (scale bar, 25mm).

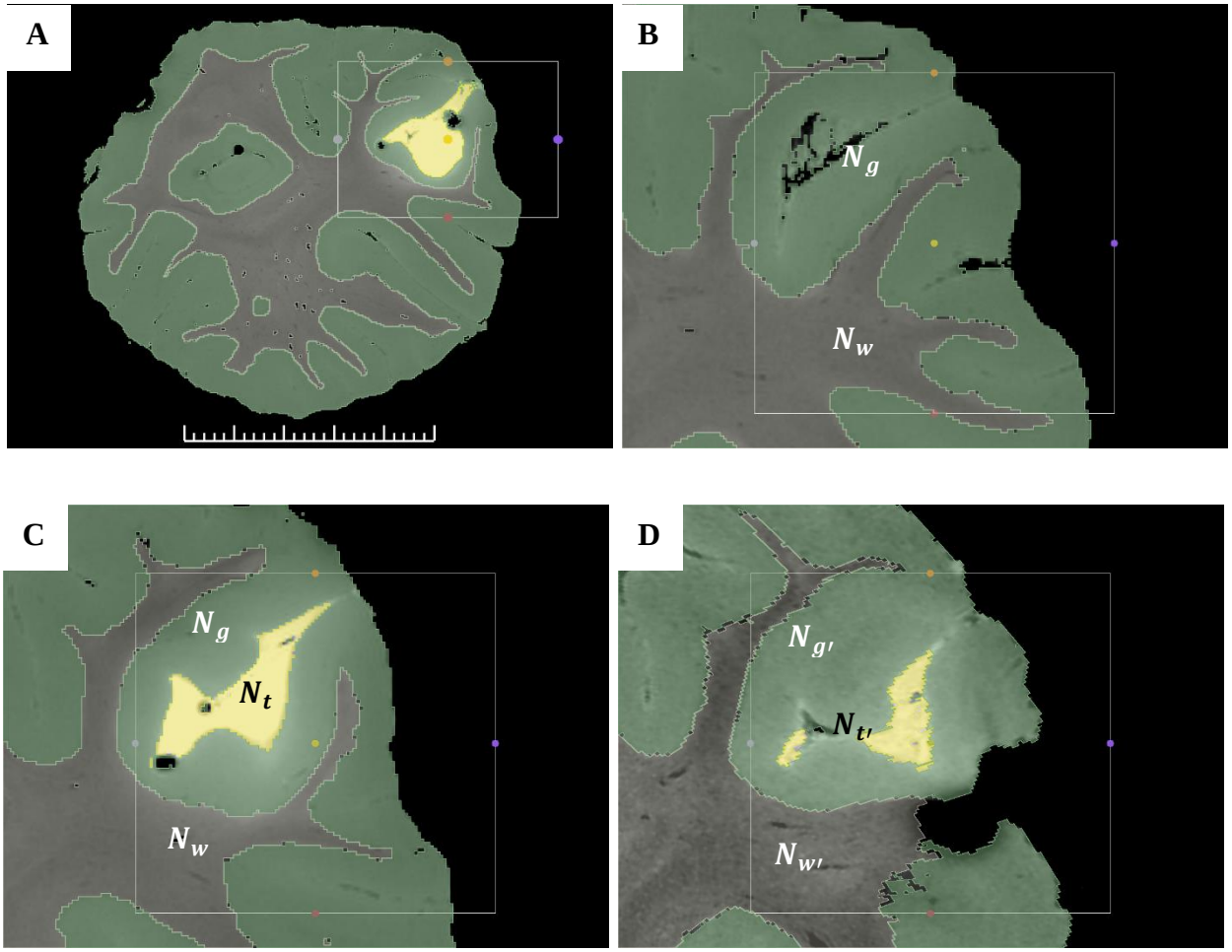

Figure 6: Coronal 7-Tesla MRIs of segmented calf brain hemisphere (Group 2, calf brain hemisphere 1) labelled with quantifiable variables.

(A) Baseline coronal segmented image of calf brain hemisphere (scale bar, 25mm) containing irregular tumor outlined within an outlined region of interest (ROI). (B) Detailed view of the segmented image with ROI in which no tumor is visualized with quantifiable grey (N_g) and white matter (N_w) tissue regions. (C) Detailed view of baseline segmented image with ROI and quantifiable grey (N_g) , white matter (N_w) tissue along with quantifiable tumor (N_t). (D) Detailed view of the postresection segmented image with ROI and quantifiable residual grey $(N_{g'})$, residual white matter $(N_{w'})$ along with residual tumor $(N_{t'})$.

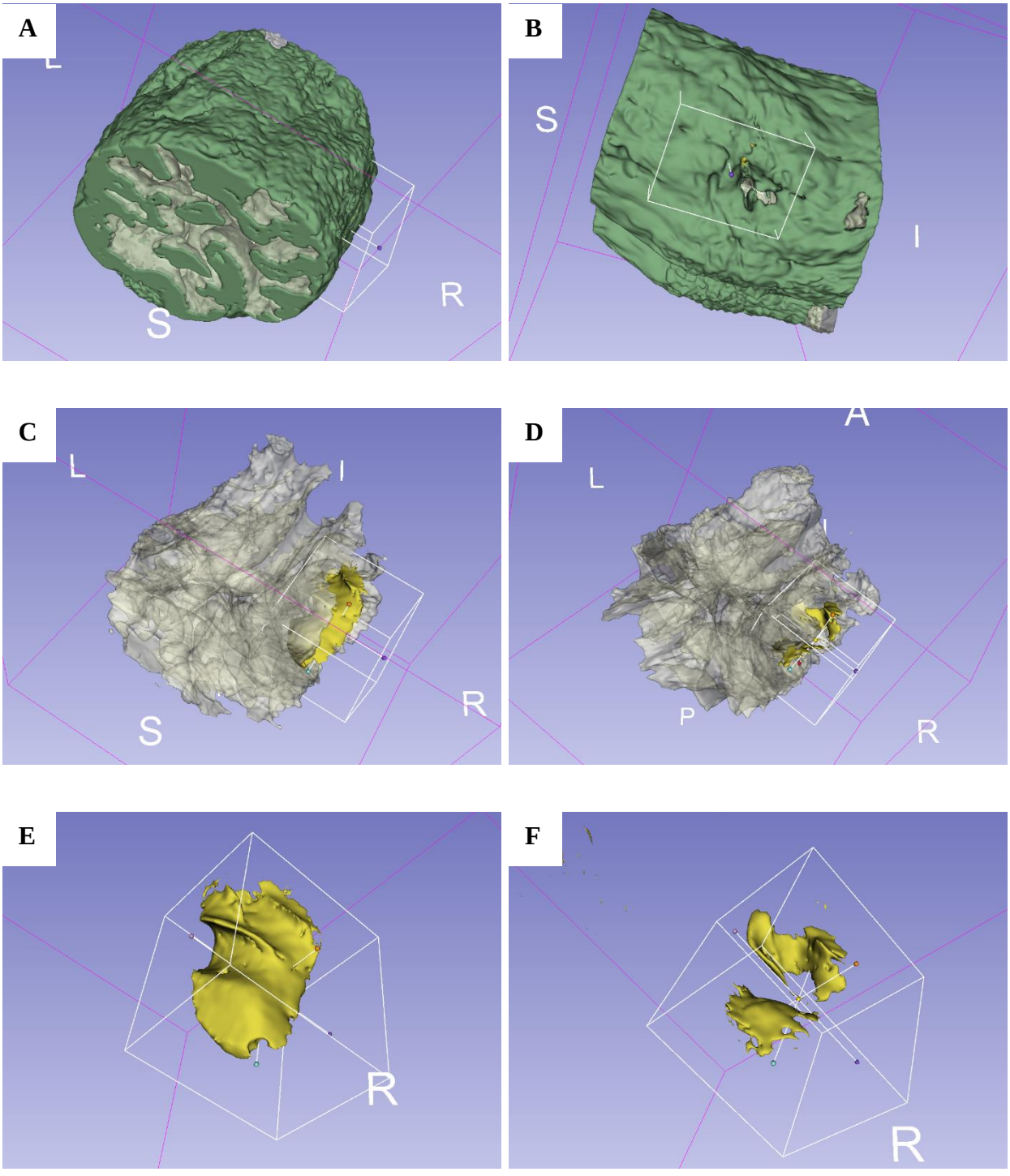

Figure 7: Baseline and postresection 3D reconstruction views of calf brain hemisphere containing alginate tumor (Group 2, calf brain hemisphere 1)

(A) Baseline 3D reconstruction of calf brain 1 demonstrating ROI containing the tumor. (B) Reconstructed 3D postresection surface view demonstrating that very small amounts of overlying grey matter were removed during tumor resection. (C) Reconstructed baseline 3D view containing the ROI in which grey matter has been removed to allow visualization of white matter (white) and tumor (yellow). (D) Reconstructed postresection 3D view containing the ROI outlining the position and shape of the residual tumor (yellow). (E) Reconstructed baseline 3D view containing the ROI in which the grey and white matter have been removed allowing visualization of the irregular shape of the tumor (yellow). (F) Reconstructed postresection 3D view containing the ROI in which the grey and white matter have been removed, allowing visualization of the two areas of residual tumor (yellow). The white box, which outlines the ROI, was kept constant between the baseline and postresection 3D views.

VIDEOS

Video 1. View of Scrolling Coronal MRI slices of brain 1 and 3 of Group 2

This video features two brains from Group 2 to demonstrate the use of such video to determine the result of an alginate tumor resection. Brain 1 was used to illustrate subtotal alginate tumor resection and brain 3 was used to illustrate complete alginate tumor resection. These brains are viewed by scrolling along their coronal axis. Left: baseline coronal brain images containing alginate tumors. Right; postresection coronal brain images.